Supporting Information

Degradation Pathways of a highly active iron(III) tetra-NHC Epoxidation Catalyst

Florian Dyckhoff, Jonas F. Schlagintweit, Marco A. Bernd, Christian H. G. Jakob, Tim P. Schlachta, Benjamin J. Hofmann, Robert M. Reich and Fritz E. Kühn*

Molecular Catalysis, Catalysis Research Center and Department of Chemistry, Technische Universität München, Lichtenbergstrasse 4, D-85748 Garching bei München, Germany.

[*] Corresponding author: Prof. Dr. Fritz E. Kühn, E-Mail: fritz.kuehn@ch.tum.de

Table of Contents

1. Effects of bases on 2, 2-tBuCN and 2-PhCN – Catalysis and UV/vis Spectroscopy

All batch and time-dependent reactions were conducted in a cryostat (Julabo FP-50) with a total reaction volume of 2.0 mL. The catalyst (0.05 mol%, 0.067 µmol) was added from a preformed stock solution (4.0 mg/mL in the respective nitrile, *i.e.* acetonitrile, *tert*-butylnitrile or benzonitrile) according to the appropriate stoichiometry to a solution of *cis*-cyclooctene (100 mol%, 134.5 µmol), the respective additive (0.5 mol%, 0.67 µmol) and H_2O_2 (150 mol%, 202 µmol, 50% solution in H_2O) in the appropriate solvent. The reaction was initiated upon addition of H_2O_2. The reaction was aborted by adding electrolytically precipitated activated MnO_2 as a H_2O_2 decomposition agent. After filtration over activated neutral alumina, two GC samples were prepared for each experiment and data point using 200 µL filtrate, 500 µL external standard (*p*-xylene, 4.0 mg/mL in *i*-PrOH) and 800 µL n-hexane, respectively. Control experiments without catalyst and additive were performed as a reference for all reactions.

UV/vis spectra were recorded on an Agilent Technologies Cary 60 UV-Vis spectrophotometer at 20°C. Solutions of 1.0 eq. **2**, **2-^{t}BuCN** and **2-PhCN** with an initial concentration of 1.5×10^{-4} M in the respective nitrile (*i.e.* acetonitrile, *tert*-butylnitrile and benzonitrile) are treated with 10 eq. NEt_3 in air. All solutions were stirred continuously during each experiment.

Table S1. Effects of solvent and different bases on the performance of catalysts **2-MeCN**, **2-^{t}BuCN** and **2-PhCN** in the epoxidation of *cis*-cyclooctene.

entry	catalyst	solvent	base	yield[a] (%)	TON
1	**2-MeCN**	MeCN	-	37	740
2	**2-MeCN**	MeCN	NEt_3	< 1	< 10
3	**2-MeCN**	MeCN	BDAN[e]	-	-
4	**2-MeCN**	acetone[b]	-	19	380
5	**2-MeCN**	acetone[b]	NEt_3	< 1	< 10
6	**2-MeCN**	acetone[b]	BDAN[e]	-	-
7	**2-^{t}BuCN**	^{t}BuCN	-	2	30
8	**2-^{t}BuCN**	^{t}BuCN	NEt_3	< 1	< 10
9	**2-^{t}BuCN**	acetone[c]	-	7	140
10	**2-^{t}BuCN**	acetone[c]	NEt_3	< 1	< 10
11	**2-^{t}BuCN**	acetone[c]	BDAN[e]	-	-
12	**2-PhCN**	PhCN	-	< 1	< 10
13	**2-PhCN**	PhCN	NEt_3	< 1	< 10
14	**2-PhCN**	acetone[d]	-	< 1	< 10
15	**2-PhCN**	acetone[d]	NEt_3	< 1	< 10
16	**2-PhCN**	acetone[d]	BDAN[e]	-	-
17	**-**	MeCN	-	-	-
18	**-**	acetone[d]	-	-	-
19	**-**	MeCN	NEt_3	-	-
20	**-**	MeCN	BDAN[e]	-	-

Reaction conditions: *cis*-cyclooctene (134.5 µmol, 100 mol%), H_2O_2 (202 µmol, 150 mol%), catalyst (0.067 µmol, 0.05 mol%), base (0.67 µmol, 0.5 mol%); T = 20°C. [a] All yields were determined *via* GC-FID after a reaction time of 2 h, selectivity >99% for all reactions; [b] 95 vol.% acetone in MeCN; [c] 95 vol.% acetone in ^{t}BuCN; [d] 95 vol.% acetone in PhCN; [e] 1,8-Bis(dimethylamino)naphthalene.

In order to avoid the reduction of the active Fe^{III} catalyst, two analogues **2-^{t}BuCN** and **2-PhCN** of **2** are synthesized, exchanging both apical acetonitrile ligands of **2** with *tert*-butylnitrile and benzonitrile, respectively (Figure S1). These nitriles are far less prone to oxidation due to the absence of C-H bonds in

α-position to the nitrile group. Therefore, reduction of the respective Fe^{III} catalysts in presence of a base would be impeded if the reaction is conducted applying the respective nitrile (*i.e.* ^{t}BuCN or PhCN) or a non-oxidisable substance (*e.g.* acetone) as solvent enabling NEt_3/BDAN to potentially unfold its H^+ scavenging properties during a catalytic epoxidation reaction, in the case of ligand protonation being part of a crucial decomposition pathway.

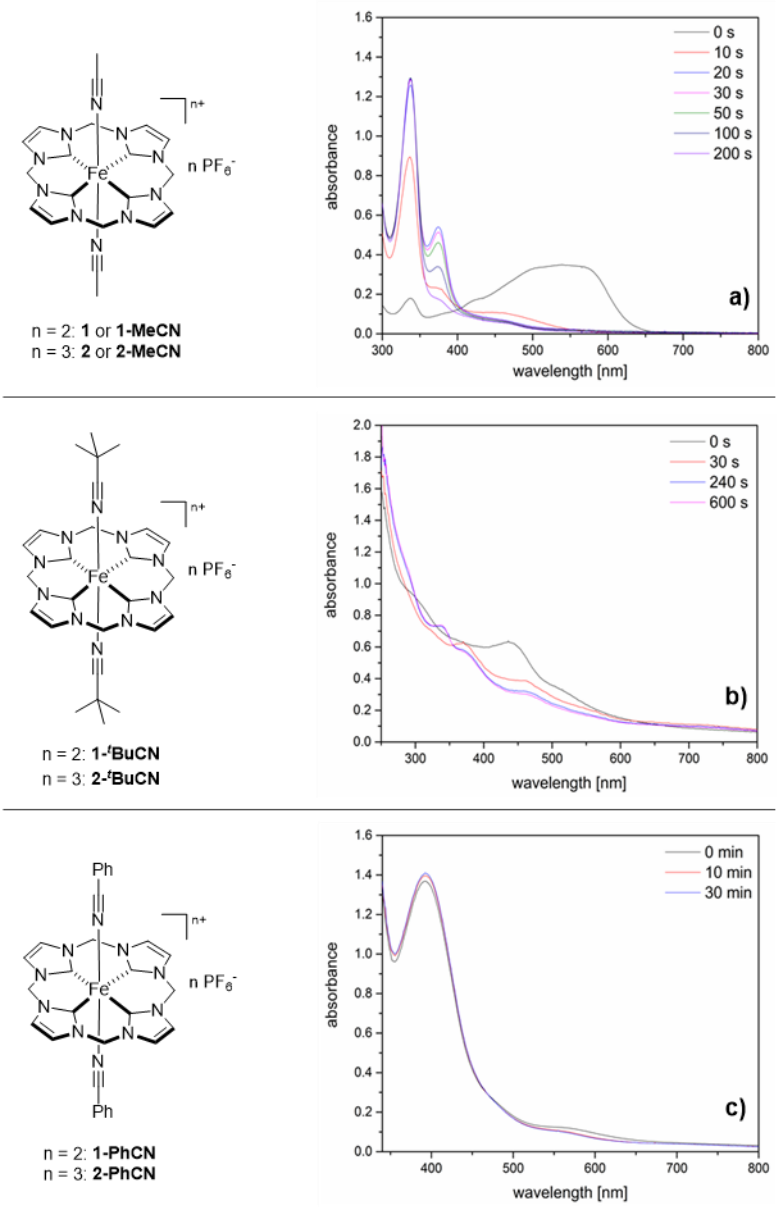

Figure S1. UV/vis kinetics of the reaction of **2**(a)/**2-^{t}BuCN**(b)/**2-PhCN**(c) (t = 0 s) with 10 eq. NEt_3. a) Due to coordination of NEt_3 to the Fe^{III} centre the broad absorption maximum of **2** (Fe^{III}; around 400 nm to 650 nm) is blue-shifted. Formation of **1** (Fe^{II}; λ_{max} = 337 nm) and 3 (Fe^{III}-O-Fe^{III}; λ_{max} = 376 nm) occurs instantly after addition of the base. As reported previously, **3** slowly decays under formation **1** due to oxidation of MeCN. b) Due to coordination of NEt_3 to the Fe^{III} centre the broad absorption maximum of **2-^{t}BuCN** (Fe^{III}; around 400 nm to 600 nm) is blue-shifted. Formation of **3** (λ_{max} = 376 nm) and **1-^{t}BuCN** (Fe^{II}; λ_{max} = 341 nm) occurs after addition of the base, however at a significantly slower rate, when compared to starting with **2**. Again, **3** slowly decays under formation of **1-^{t}BuCN**. c) After addition of base, even after 30 min no significant amounts of **2-PhCN** (λ_{max} = 394 nm) react.

The resilience of ^{t}BuCN and PhCN to be oxidised under basic conditions and, in consequence, the stability of the respective Fe^{III} complexes **2-^{t}BuCN** and **2-PhCN** were investigated *via* UV/vis spectroscopic

measurements and put in reference to the behaviour of **2-MeCN** in acetonitrile. Time-dependent recordings reveal an almost instantaneous transformation of Fe^{III} complex **2-MeCN** in acetonitrile to both the respective Fe^{II} complex **1** and Fe^{III}-O-Fe^{III} complex **3** upon addition of 10 eq. of NEt_3 under ambient conditions (Figure S1, a), as already demonstrated by ^{1}H-NMR (Figure S2). Over a subsequent period of 5 min complex **3** is reduced to **1** without any remaining traces of an Fe^{III} compound. This transformation of **3** to **1** in acetonitrile was reported previously, even in absence of a base, and is a consequence of acetonitrile oxidation under ambient conditions. In contrast, reduction of **2-^{t}BuCN** to its respective Fe^{II} derivative in *tert*-butylnitrile occurs considerably slower - within minutes - under otherwise identical reaction conditions (Figure S1, b). In the reaction of NEt_3 with **2-PhCN** no substantial transformation of the Fe^{III} complex is observed over a period of 30 min (Figure S1, c). Therefore, the targeted effect of using sterically and electronically hindered nitriles to significantly impede their oxidation and consequentially the reduction of the respective Fe^{III} complexes was achieved. However, employing **2-^{t}BuCN** and **2-PhCN** as catalysts (0.05 mol%) in epoxidation reactions using the respective nitriles as solvent affords only small amounts of epoxide (Table S1). Both *tert*-butylnitrile and benzonitrile appear to exhibit a considerably stronger coordination to the Fe-centre, resulting in a drastically decreased performance of both catalysts. An influence of the nitriles on the electronic properties of the Fe-centres can largely be excluded due to their almost identical half-cell potentials in comparison to **2**. Replacing 95 vol.% of the nitrile solvents with an – in this relation – non-coordinating and non-oxidisable solvent (*i.e.* acetone) in order to ensure comparability increases the TON of **2-^{t}BuCN** from *ca.* 30 to 140, however, no performance improvements of **2-PhCN** are observed. Adding NEt_3 or BDAN to the reaction results in almost complete deactivation of all catalysts **2-MeCN**, **2-^{t}BuCN** and **2-PhCN** and only traces of epoxide formation after a reaction time of 2 h, regardless of applied solvent. Despite a base most likely having an impairing impact on the rate constant of iron-oxo active species formation, an improved stability should be visible in case of ligand protonation being involved in a decisive catalyst degradation pathway.

2. ^{1}H-NMR Spectroscopic Studies

Reactivity studies of the influence of a base (*i.e.* NEt_3 and 1,8-Bis(dimethylamino)naphthalene) on Fe^{III} complex **2** were monitored *via* ^{1}H-NMR spectroscopy. The respective base (1.6 µmol) was added from a preformed solution in CD_3CN to a solution of complex **2** (1.6 µmol, 461 µL of a 3.1 mg/mL solution in CD_3CN) and the standard (EtOAc, 6.4 µmol). An instantaneous colour change from purple to greenish-yellow indicated formation of compounds **1** and **3**, as confirmed by the ^{1}H-NMR spectra in Figure S2.

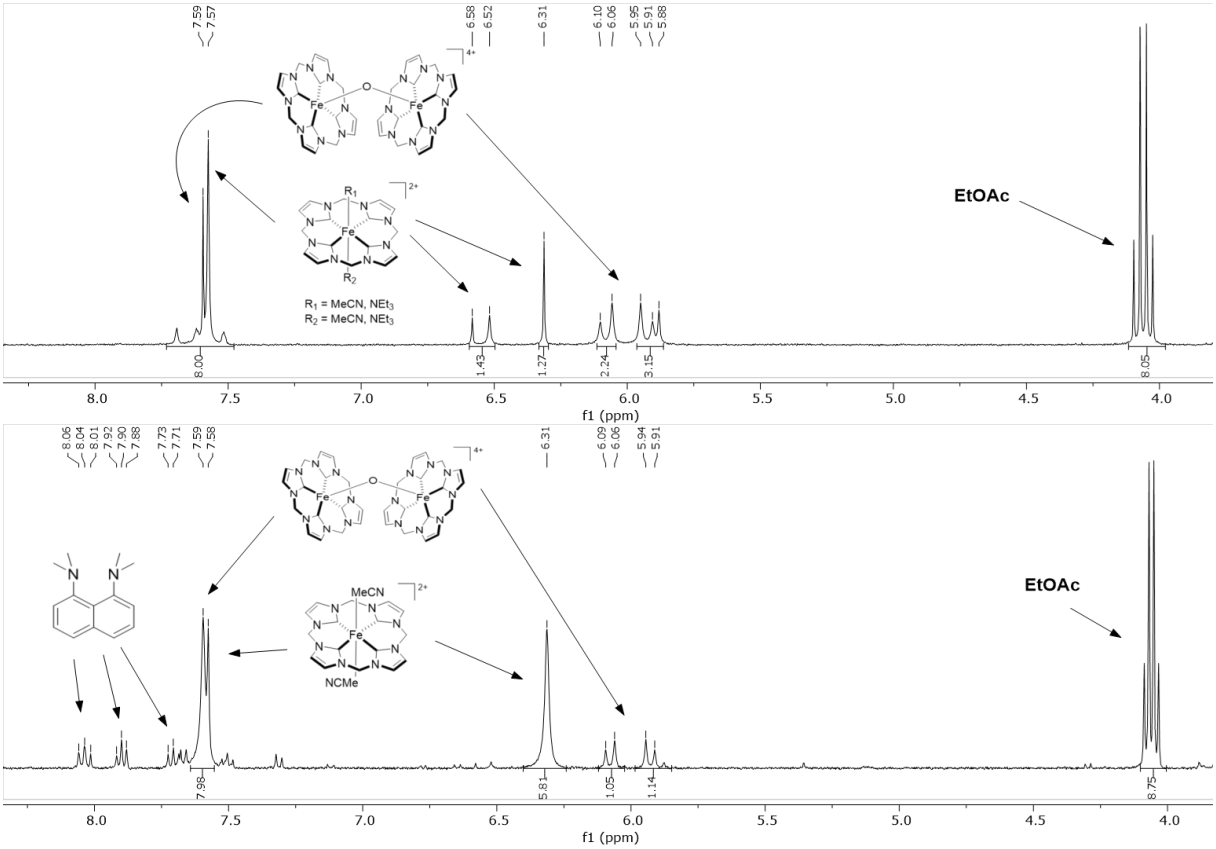

Figure S2. ^{1}H-NMR spectra of the reaction of complex **2** (1.6 µmol) with a coordinating base (*i.e.* NEt_3, 1.6 µmol, *top*) and a non-coordinating base (*i.e.* 1,8-Bis(dimethylamino)naphthalene, 1.6 µmol, *bottom*) in CD_3CN. EtOAc was applied as a standard for both reactions.

An otherwise identical experiment with NEt_3 as a base revealed acetonitrile to be the reagent to be oxidised in turn of Fe^{III} reduction by replacing 5 vol.% of CD_3CN with CH_3CN. A distinctive formaldehyde signal at 9.31 ppm evidences the formation of glycolonitrile, which decays to formaldehyde and hydrogen cyanide under basic conditions (Figure S3).

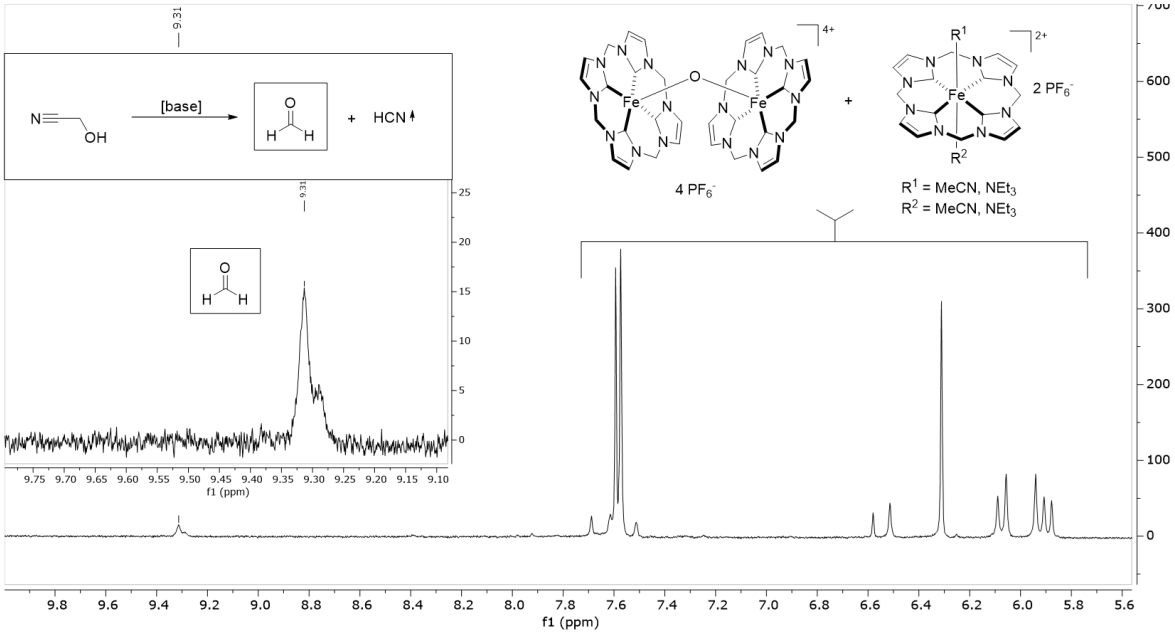

Figure S3. ^{1}H-NMR spectrum of the reaction of complex **2** (1.6 µmol) with NEt_3 (3.2 µmol) in CD_3CN (5 vol.% CH_3CN). The appearance of a formaldehyde signal at 9.31 ppm indicates the oxidation of acetonitrile to glycolonitrile in turn of the reduction of Fe^{III} (**2**) to Fe^{II} (**1**).

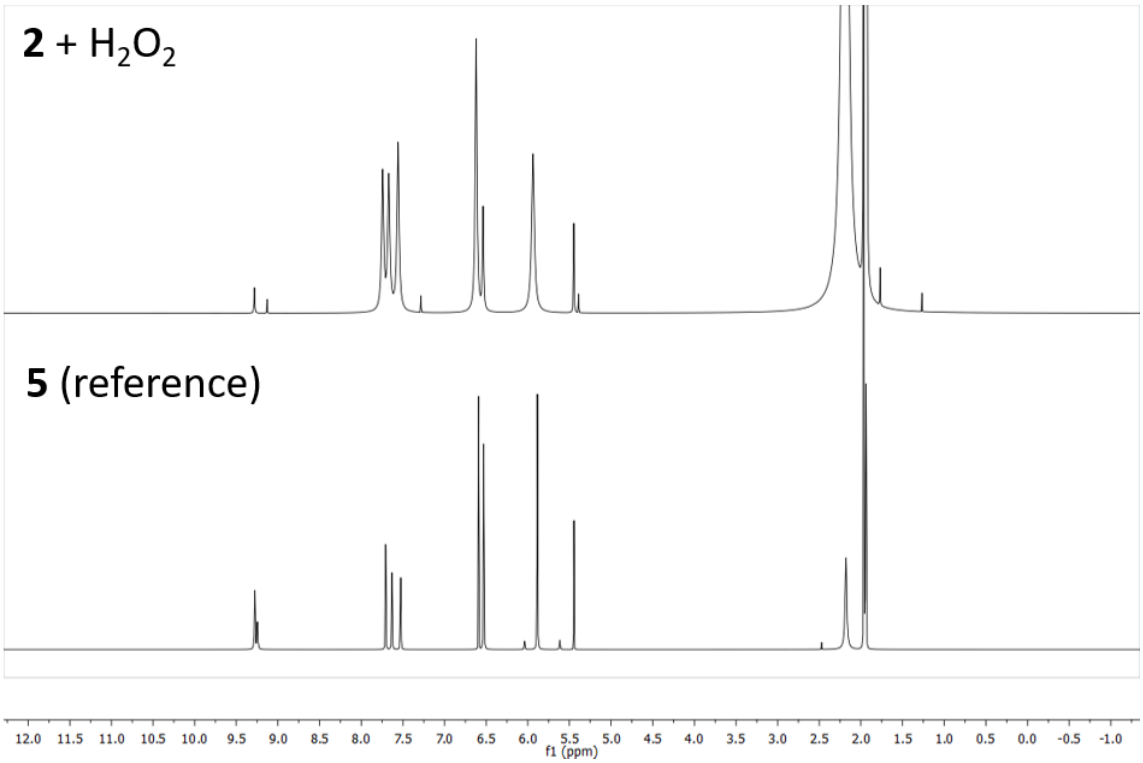

Figure S4. ^{1}H-NMR spectrum obtained after reaction of **2** with 10 eq. H_2O_2 and filtration through Al_2O_3 (twice) in CD_3CN (*top*). All main signals of the mono-oxidised and protonated tetra-NHC Ligand **5** (reference, *bottom*) are observed.

3. Synthesis and Characterization of compound 2-d_8

Materials and Methods

Unless otherwise stated, all manipulations were performed under an argon atmosphere using standard Schlenk and glovebox techniques. Solvents were obtained water- and oxygen-free from a MBraun solvent purification system and stored over molecular sieves (3 Å). DMSO was dried being refluxed over CaH_2 and distilled prior to being stored over a molecular sieve (4 Å), MeCN-d_3 was refluxed over phosphorus pentoxide and distilled prior to use. [Fe(btsa)$_2$(THF)][1] and thianthrenyl hexafluorophosphate[2] were synthesized according to literature procedures. Methylene-d_2 bis(trifluoromethansulfonate) (Me-d_2(OTf)$_2$) was synthesized corresponding to literature,[3] utilizing paraformaldehyde-d_2 instead of regular paraformaldehyde. CD_2Cl_2 (99.80% D) was purchased from Eurisotop and paraformaldehyde-d_2 (98% D) from Sigma Aldrich. All other reagents were purchased from commercial suppliers and used without further purification. NMR spectra were recorded on a Bruker Avance DPX 400 (^{1}H-NMR, 400.13 MHz; ^{13}C-NMR, 100.53 MHz) and Bruker Avance III 400 (^{2}H-NMR, 61 MHz). Chemical shifts are reported relative to the residual signal of the deuterated solvent. For ^{2}H-NMR spectra, chemical shifts are reported relative to the added standard of deuterated solvent diluted in the equivalent amount of non-deuterated solvent. Elemental analyses (C/H/N/S) were performed by the microanalytical laboratory at Technische Universität München. The calculated results for the elemental analysis of deuterated compounds are stated as non-deuterated components, as the detection is performed *via* gas chromatography with subsequent thermal conduction. With this setup, no differentiation can be made between the proton and deuterium content. Therefore, this method is only liable to confirm the absence of major contaminations. Electrospray ionization mass spectrometry (ESI-MS) data were acquired on a Thermo Fisher Ultimate 3000, high resolution mass spectrometry (HR-ESI-MS) data were acquired on a Thermo Fisher Exactive Plus Orbitrap. CV measurements were recorded using a Metrohm Autolab potentiostat employing a gastight three-electrode cell under an argon atmosphere. A glassy carbon electrode was used as the working electrode and polished before each measurement. A graphite stick was used as the counter electrode. The potential was measured against Ag/AgCl (3.4 M KCl) with a scan rate of 100 mV/s and ferrocene was applied as an internal standard. Tetrabutylammonium hexafluorophosphate (100 mM in MeCN) was used as the electrolyte. The concentration of the complexes was about 5 mM.

Synthetic Procedures

Sodium imidazolide (**NaIm**)

Imidazole (20.0 g, 294 mmol, 1.00 eq.) is melted at 110 °C in an open round bottom flask and powdered NaOH (11.2 g, 279 mmol, 0.95 eq.) is slowly added. The reaction temperature is maintained at 110 °C for 4 h under stirring, allowing the generated water steam to leave the reaction vessel. After cooling to room temperature, the resulting yellow solid is subsequently washed with water (5 mL), THF (2x 50 mL) and pentane (50 mL). After drying in *vacuo*, the product is obtained as a pale orange solid in 86% yield (21.6 g, 240 mmol)

^{1}H-NMR (400 MHz, DMSO, 296 K): δ(ppm) = 7.13 (s, 1H, N-C*H*-N), 6.70 (s, 2H, N-C*H*-C).

These data are in alignment with literature.[4]

Elemental analysis: calc. for $C_3H_3N_2Na$: C 40.01; H 3.36; N 31.11; S 0.00

found: C 39.98; H 3.44; N 31.28; S 0.00.

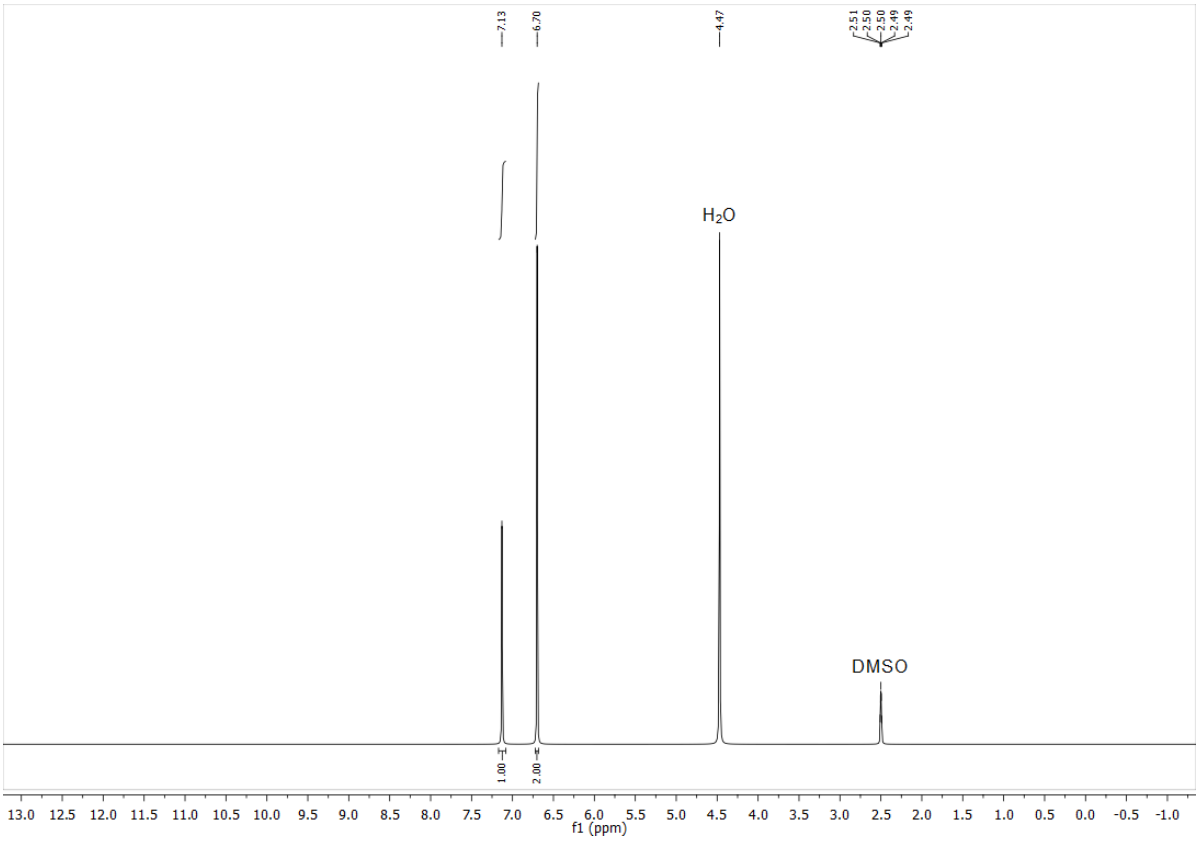

Figure S5. ^{1}H-NMR spectrum of **NaIm** in DMSO-d_6, the water signal is downfield shifted due to the alkaline character of **NaIm**.

Di(imidazol-1-yl)methane-d_2 (**Im$_2$Me-d_2**)

The synthesis is based upon a modified method from literature.[5]

To minimize a potential H-D exchange, imidazole is deprotonated prior conversion to avoid applying an external base and the reaction is performed using a dry solvent. **NaIm** is not soluble in MeCN, therefore the reaction is performed in dry DMSO.

In the ^{1}H-NMR spectrum of $CDCl_3$, all non-deuterated signals are in alignment with literature,[6] confirming the identity of the compound. Further discussion will be based on NMR spectra measured in CD_3CN. The small signal at 6.06 ppm with an intensity of 0.01 originates from the residual proton content. This signal is a triplet due to a $^2J_{H\text{-}D}$ coupling, therefore the proton signal originates from a partly deuterated species. The content of deuteration can therefore be calculated to be >99%.

The ^{13}C-NMR spectrum shows four signals, the signal at 56.09 ppm originates from the deuterated methylene bridge and shows a triplet of triplet splitting with a coupling constant of 23.6 Hz due to $^1J_{C\text{-}D}$ coupling of two deuterium atoms with the ^{13}C.

The ^{2}H-NMR shows one signal for the deuterated methylene bridge, which is in alignment in terms of chemical shift for the corresponding non-deuterated species.

The detected mass signal in ESI-MS is two atomic units heavier than its non-deuterated counterpart in literature, which further confirms the successful synthesis.

NaIm (6.53 g, 72.5 mmol, 1.0 eq.) is dissolved in 55 mL of dry DMSO. CD_2Cl_2 (8.1 mL, 9.45 g, 108.72 mmol, 1.75 eq.) is added and the mixture is stirred for 19 h at 40 °C. DMSO is removed from the resulting orange suspension *via* vacuum distillation and the residue is suspended in 40 mL acetonitrile. After filtration and washing of the solid four times with 20 mL acetonitrile, the combined organic solutions are reduced to 20 mL volume. Upon addition of diethyl ether, a pink solid precipitates. The crude product is dissolved in 70 mL acetonitrile and filtered over silica, using 100 mL acetonitrile as an eluent. The solvent is removed in *vacuo*, the resulting white solid re-dissolved in 20 mL acetone and precipitated with 40 mL n-pentane. The product is obtained as a white solid in 75% yield (4.09 g, 27.2 mmol). The deuterium content at the methylene bridges is determined to be 99.9% *via* ^{1}H-NMR.

^{1}H-NMR (500 MHz, $CDCl_3$) δ(ppm) = 7.64 (s, 2H, N-C*H*-N), 7.09 (s, 2H, N-C*H*-CH), 6.98 (t, *J* = 1.2 Hz, 2H, N-C*H*-CH), 5.98 (t, residual H, $^2J_{2H\text{-}1H}$ = 1.81 Hz, -C*D*$_2$-).

^{1}H-NMR (500 MHz, CD_3CN) δ(ppm) = 7.73 (s, 2H, N-C*H*-N), 7.18 (s, 2H, N-C*H*-CH), 6.95 (s, 2H, N-C*H*-CH), 6.06 (t, residual H, $^2J_{2H\text{-}1H}$ = 2.1 Hz, -C*D*$_2$-).

^{13}C-NMR (126 MHz, CD_3CN) δ(ppm) = 138.06 (N-*C*H-N), 130.71 (CH-*C*H-N), 119.56 (N-*C*H-CH), 56.09 (tt, $^1J_{2H\text{-}13C}$ = 23.6 Hz, -*C*D$_2$-).

^{2}H-NMR (61 MHz, CH_3CN) δ(ppm) = 6.05 (s, 2D, -*CD*$_2$-)

ESI-MS: m/z [**Im$_2$Me-*d*$_2$** +1H$^+$]$^+$ calc: 151.09, found: 150.93

Elemental analysis: anal. calc. for $C_7H_8N_4$: C 56.74; H 5.44; N 37.81; S 0.00
found: C 55.67; H 5.28; N 36.76; S 0.00.

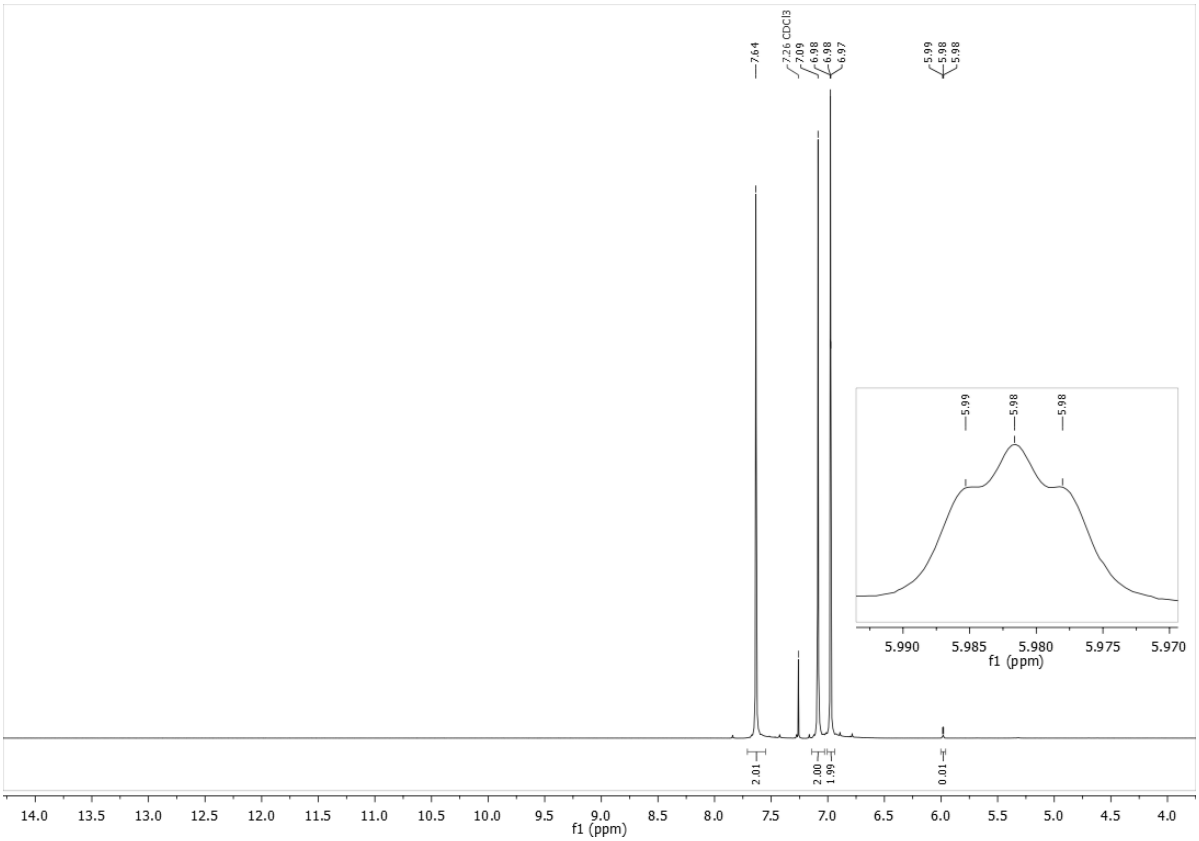

Figure S6. ^{1}H-NMR of **Im$_2$Me-*d$_2$*** in $CDCl_3$, signals for non-deuterated regions are in alignment with literature,[5] no loss of deuterium content is visible.

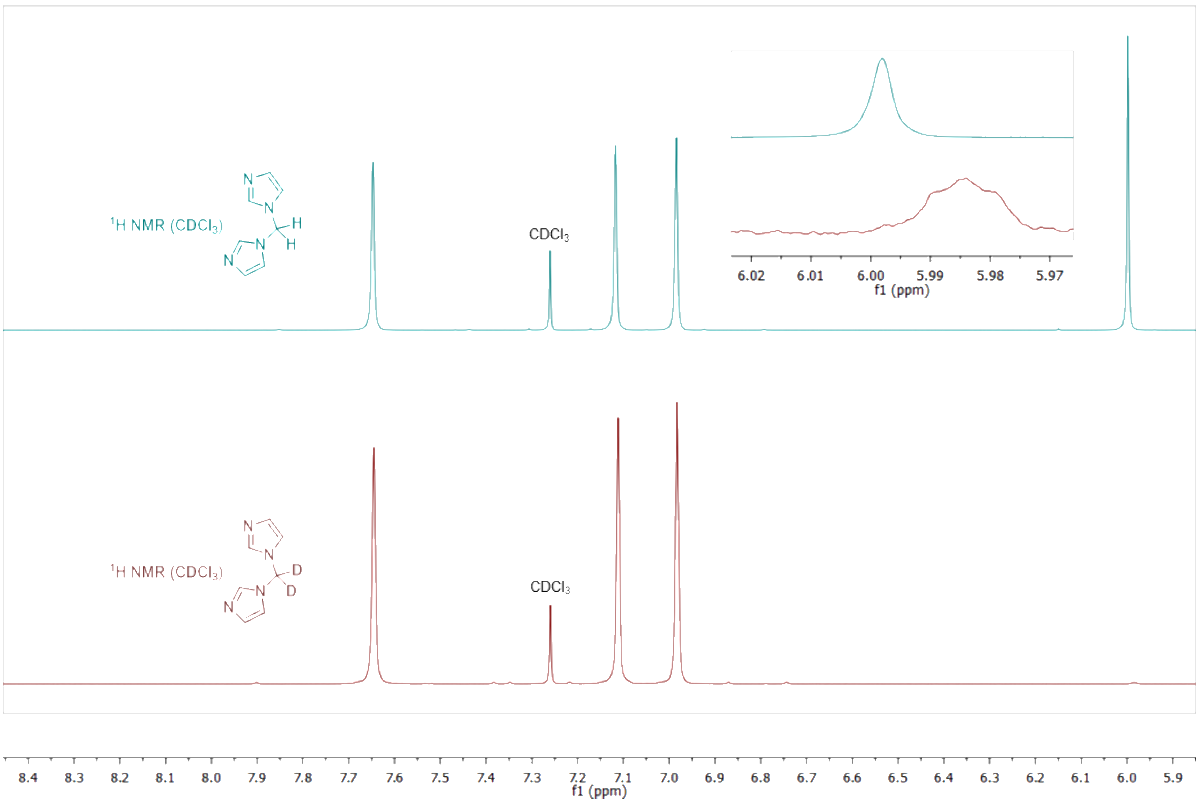

Figure S7. Comparative ^{1}H and ^{2}H-NMR spectra of **Im$_2$Me-*d$_2$*** and its non-deuterated analogue in $CDCl_3$.

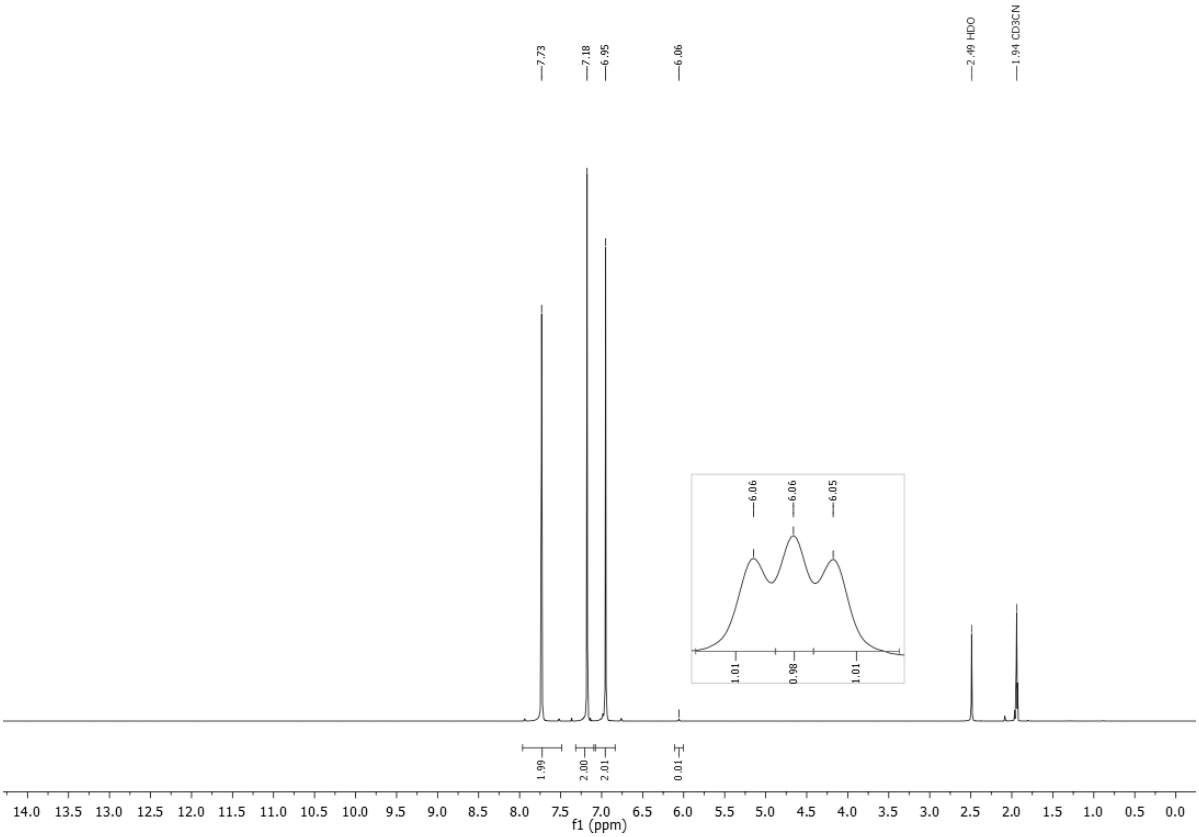

Figure S8. ^{1}H-NMR of **Im$_2$Me-*d$_2$*** in CD_3CN, no loss of deuterium content is visible.

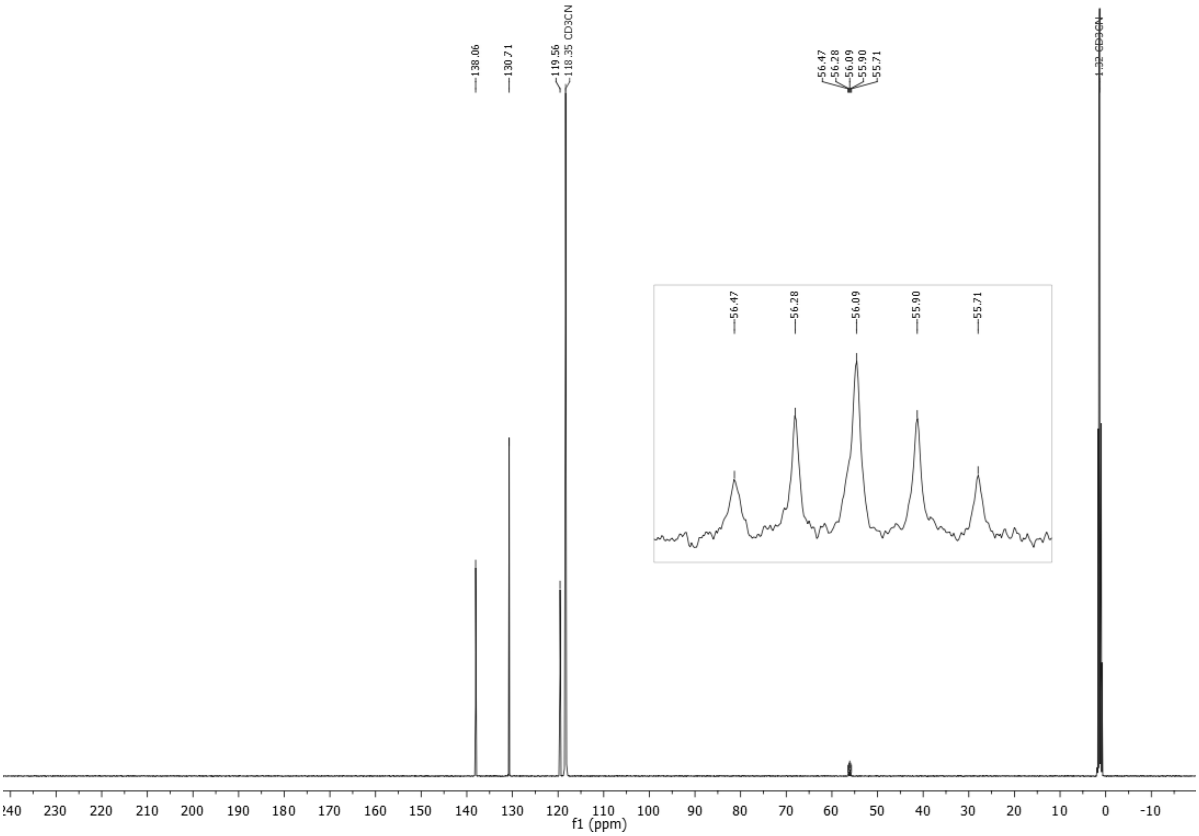

Figure S9. ^{13}C-NMR of **Im$_2$Me-*d$_2$*** in CD_3CN, the presence of two deuterium atoms is visible due to the $^{1}J_{2H\text{-}13C}$ coupling (*tt*, 23.6 Hz) of the corresponding signal.

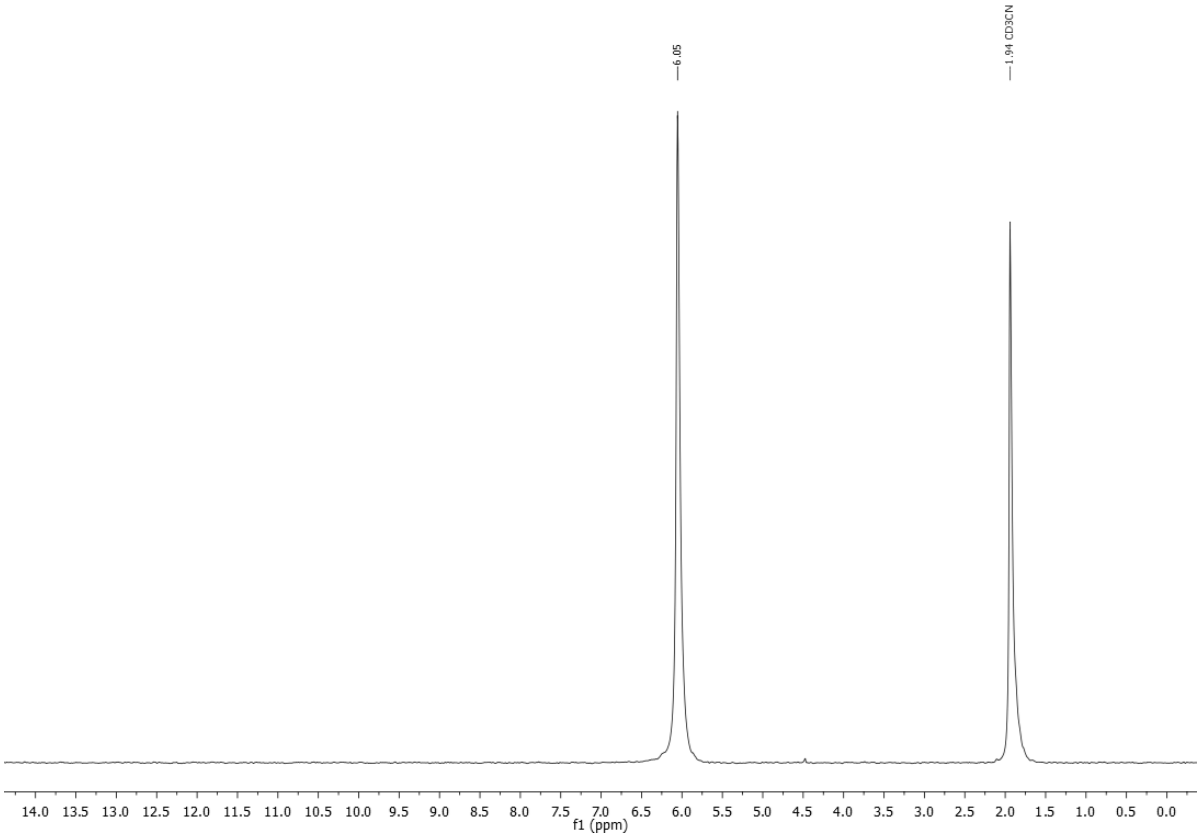

Figure S10. ^{2}H-NMR of **Im$_2$Me-*d$_2$*** in CH_3CN, the chemical shift of the deuterated methylene bridge is in alignment with literature values of a ^{1}H-NMR spectrum for the corresponding chemical environment of a non-deuterated species. CD_3CN is added as reference.

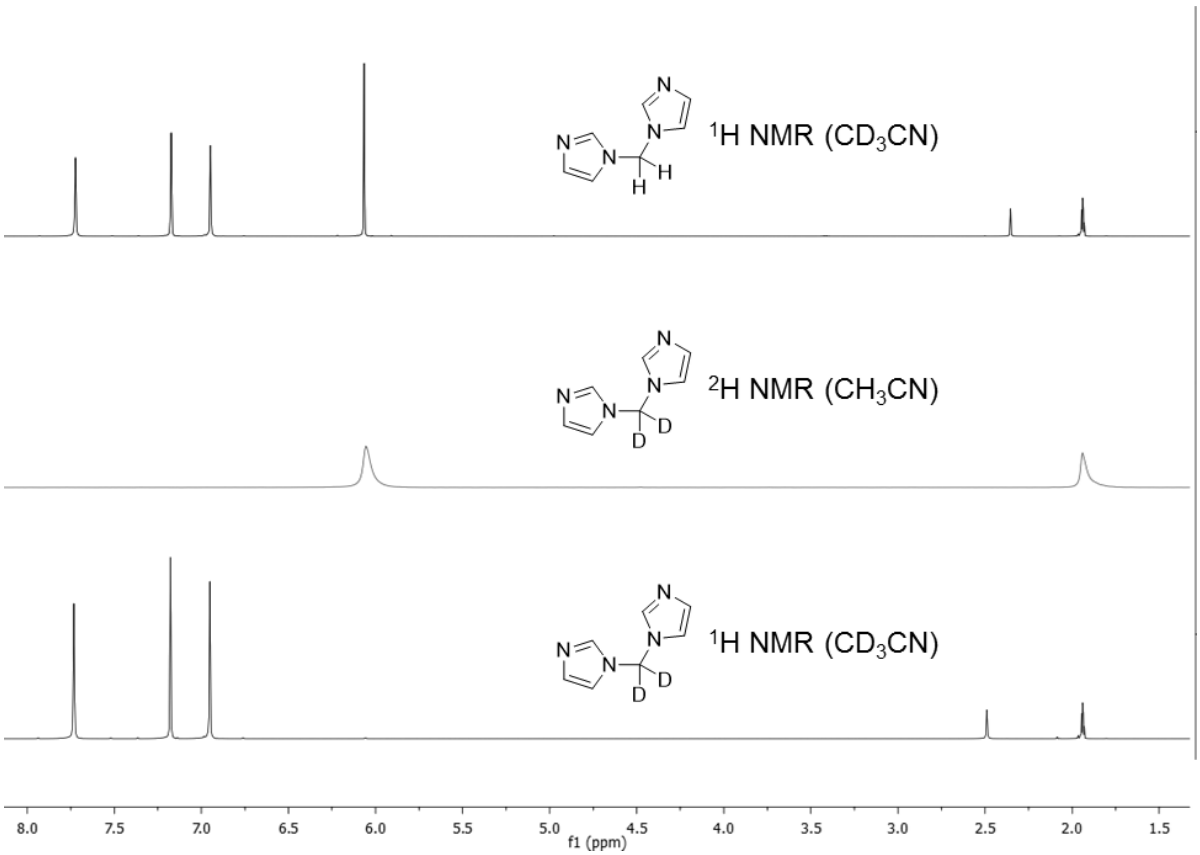

Figure S11. Comparative ^{1}H and ^{2}H-NMR spectra of **Im$_2$Me-*d$_2$*** and its non-deuterated analogue.

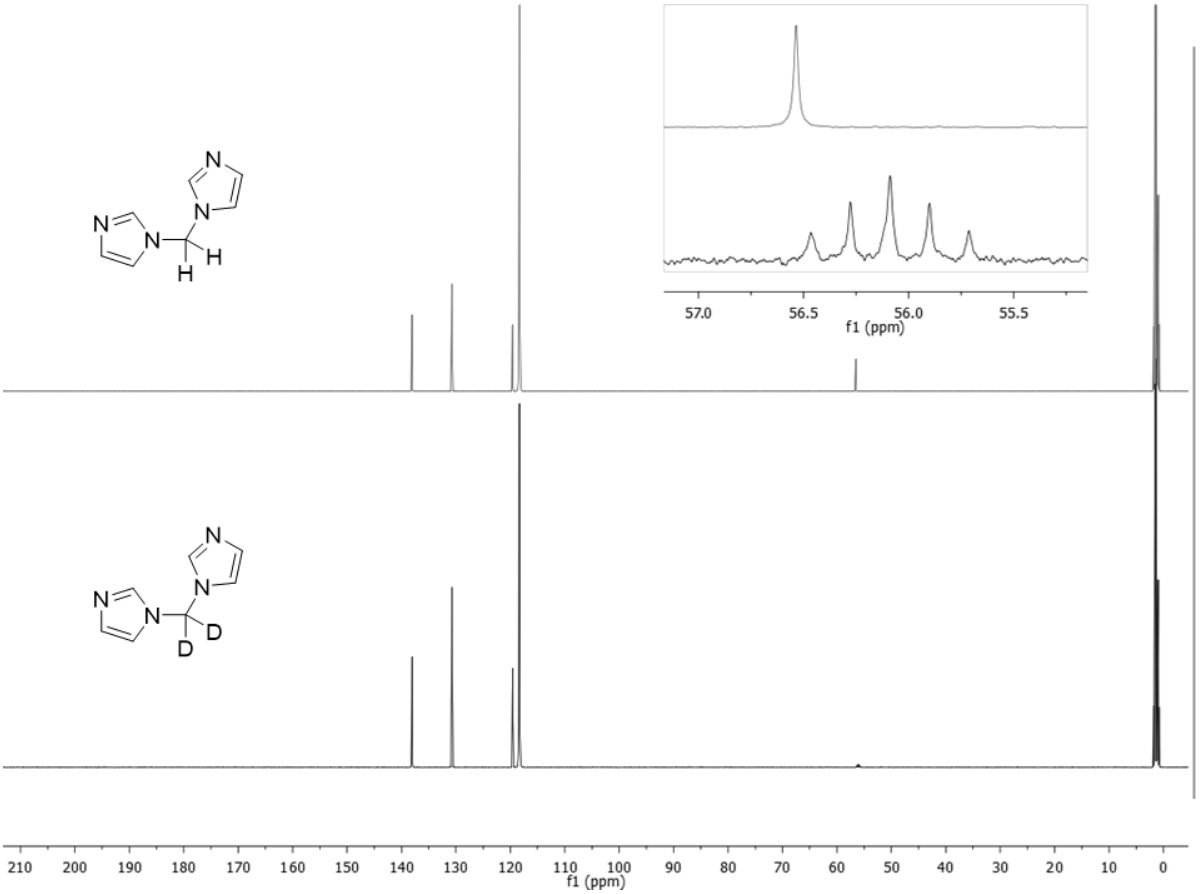

Figure S12. Comparative ^{13}C-NMR spectra of **Im$_2$Me-*d$_2$*** and its non-deuterated analogue.

Calix[4]imidazolium-*d$_8$* trifluoromethansulfonate (**L-*d$_8$* OTf**)

The synthesis is performed according to literature procedures utilizing deuterated starting materials, **Im$_2$Me-*d$_2$*** and **Me-*d$_2$*(OTf)$_2$**.[3]

The ^{1}H-NMR spectrum shows the signals of the protons at the expected chemical shift, as reported in literature. The methylene bridges' signal is also present at the expected chemical shift, but the integral suggests a deuteration content of >98%. The proton signals of the ligand precursor are not singlets, as reported in literature,[3] rather than a triplet for the imidazolium protons (9,69 ppm, t), are a triplet, due to coupling with the backbone protons (8.01 ppm, d), which in return, interact with the imidazolium protons and are present as a doublet. Additionally, a higher oligomer, consisting of six imidazole units is present. The content of this compound will be decreased during the anion exchange towards hexafluorophosphate. The ^{13}C-NMR depicts three signals of the cationic ligand structure, as well as a quartet signal deriving from the triflate anion. The signal of the methylene bridges is present as a multiplet due to $^1J_{C\text{-}D}$ coupling and possibly inversion effects of the ligand which fall within the NMR time scale and cannot be resolved.

Im$_2$Me-*d$_2$* (733.9 mg, 4.89 µmol, 2.0 eq.) is dissolved in 500 mL dry acetonitrile and cooled using an ice-bath. Me-*d$_2$*(OTf)$_2$ (1.54 g, 4.89 µmol, 2.0 eq.) are dissolved in 40 mL dry acetonitrile and slowly added towards the former solution within 1 h. The mixture is allowed to warm to room temperature and stirred for 20 h. The solvent is removed and the crude product washed twice with 2 mL acetone. After drying in *vacuo* the product is obtained

as a white solid in 72% (1.64 g, 1.76 µmol) yield. The deuterium content on the methylene bridges is determined to be >98% *via* ^{1}H-NMR.

^{1}H-NMR (500 MHz, DMSO-d_6) δ(ppm) = 9.69 (t, *J* = 1.5 Hz, 4H, N-C*H*-N), 8.01 (d, *J* = 1.6 Hz, 8H, N-C*H*-CH), 6.83 (s, residual H, -CD_2-).
^{13}C-NMR (126 MHz, DMSO-d_6) δ(ppm) = 137.84 (N-*C*H-N), 120.64 (q, *J* = 322.1 Hz, OTf), 123.61 (N-*C*H-C), 58.84 (m, -*C*D_2-).

Elemental analysis: anal. calc. for $C_{20}H_{20}F_{12}N_8O_{12}S_4$: C 26.09; H 2.19; N 12.17; S 13.93
found: C 25.80; H 2.12; N 11.80; S 13.82.

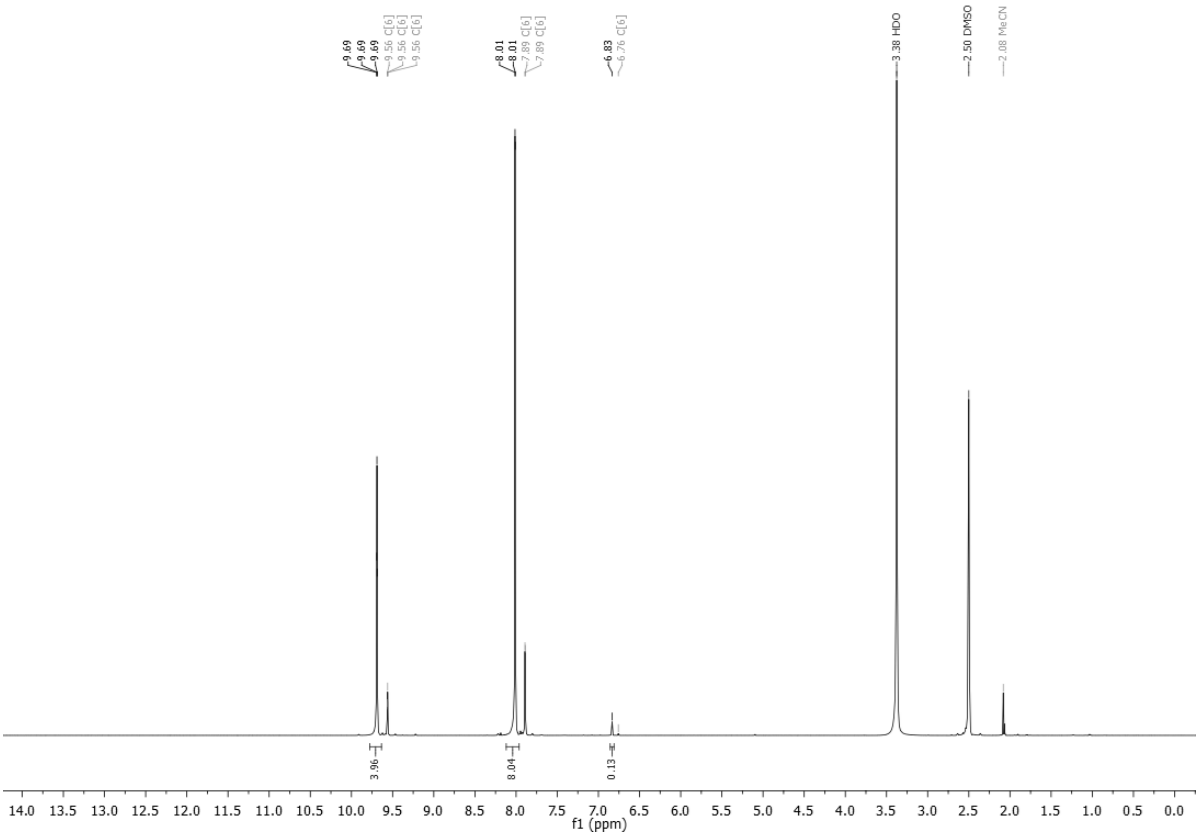

Figure S13. ^{1}H-NMR spectrum of **L-*d*$_8$ OTf** in DMSO-d_6. No loss in deuterium content is visible.

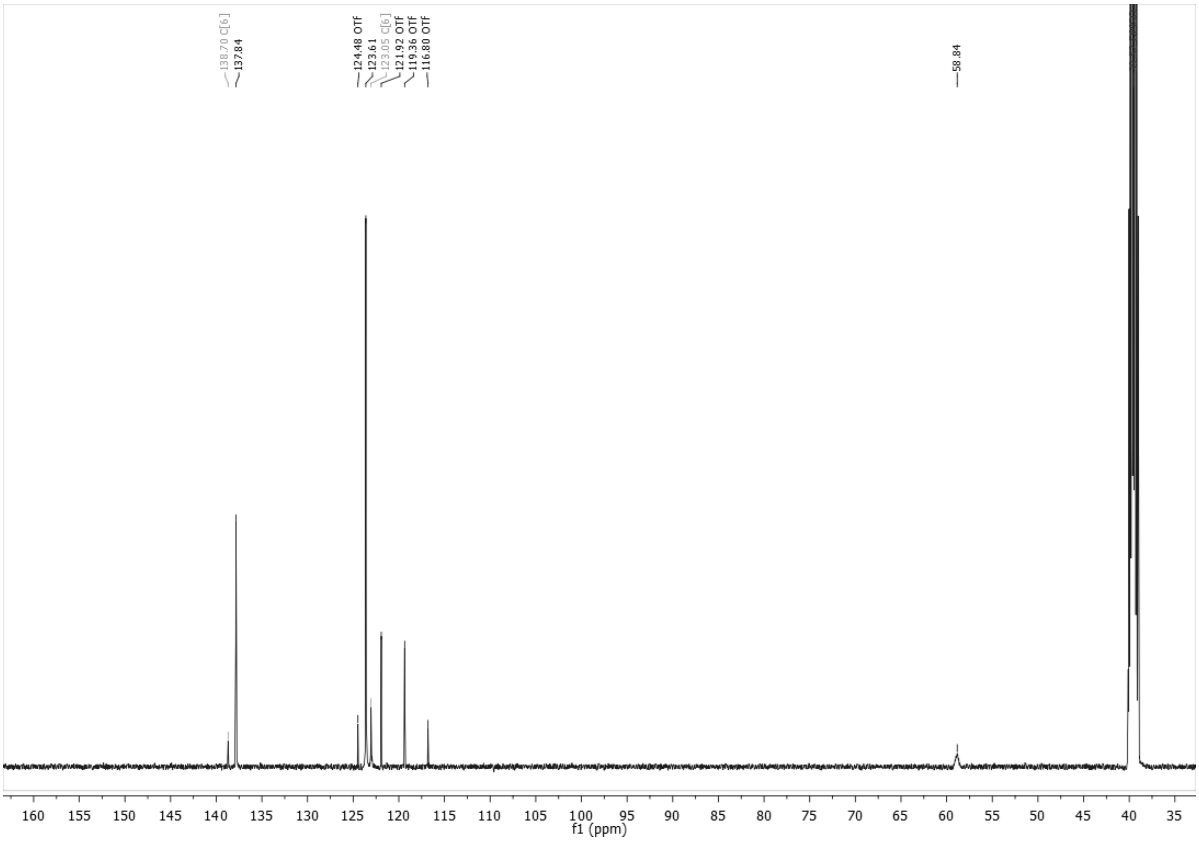

Figure S14. ^{13}C-NMR of **L-*d*$_8$ OTf**, the presence of deuterium atoms is suggested due to a multiplet at the methylene bridge, due to $^1J_{C\text{-}D}$ coupling of the corresponding signal.

Calix[4]imidazolium-*d*$_8$ trifluoromethansulfonate (**L-*d*$_8$ PF$_6$**)

The anion exchange is performed according to literature procedures for non-deuterated compounds.[3]

The ^{1}H-NMR spectra in DMSO-d$_6$ and CD$_3$CN show the expected signals for the non-deuterated region of the ligand. Still some content of the higher oligomer consisting of six imidazolium blocks is present. The content is calculated to be 5%. This impurity is negligible, as only the ligand consisting of four imidazolium blocks can effectively coordinate iron. The deuterium content of the methylene bridges does not decrease during the anion exchange and still is determined to be >98%.

The ^{13}C-NMR shows the same signals in terms of chemical shift as reported in literature and similar to **L-*d*$_8$ OTf**, with the absence of triflate signals. Interestingly, the methylene bridges signal can be resolved into a triplet of triplet multiplet pattern in CD$_3$CN, similar to the multiplicity of **Im$_2$Me-*d*$_2$**.

ESI-MS confirms the success of the synthesis and the deuteration, as the signal equals to the signal reported in literature with an increased m/z value of 8 atomic units.

The success of the anion exchange was tested *via* an unreferenced ^{19}F-NMR experiments. Here the doublet signal ($^1J_{F\text{-}P}$ = 711.4 Hz in DMSO-d$_6$; $^1J_{F\text{-}P}$ = 707.3 Hz in CD$_3$CN) for hexafluorophosphate is the main signal, whereas the singlet for triflate is almost negligible. The remaining triflate content is calculated to be approximately 0.02%.

L-*d*$_8$ OTf (1.55 g, 1.67 mmol, 1.0 eq.) is dissolved in 30 mL water and added to a solution of NH_4PF_6 (1.36 g, 8.35 mmol, 5 eq.) in 25 mL water. The precipitated white solid is isolated *via* centrifugation and washed four

times with 5 mL water. After drying in *vacuo*, the product in obtained as a white solid in 92% yield (1.40 g, 1.53 mmol) The deuterium content on the methylene bridges is determined to be >98% *via* ^{1}H-NMR.

^{1}H-NMR (500 MHz, DMSO-d_6) δ(ppm) = 9.68 (s, 4H, N-C*H*-N), 8.00 (d, *J* = 1.3 Hz, 8H, N-C*H*-C), 6.83 (s, residual H, -CD_2-).

^{13}C-NMR (126 MHz, DMSO-d_6) δ(ppm) = 137.76 (N-*C*H-N), 123.63 (N-*C*H-C) , 58.85 (m, -*C*D_2-).

^{19}F NMR (471 MHz, DMSO-d_6) δ(ppm) = -70.14 (d, $^{1}J_{31P\text{-}19F}$ = 711.4 Hz, PF_6^-), -77.73 (s, residue signal, OTf).

^{1}H-NMR (500 MHz, CD_3CN) δ(ppm) = 9.10 (s, 4H, N-C*H*-N), 7.76 (d, *J* = 1.6 Hz, 8H, N-C*H*-C), 6.63 (s, residual H, -CD_2-).

^{13}C-NMR (126 MHz, CD_3CN) δ(ppm) = 138.57 (N-*C*H-N), 125.33 (N-*C*H-C), 60.30 (tt, $^{1}J_{2H\text{-}13C}$ = 26.2 Hz, -*C*D_2-).

^{19}F NMR (471 MHz, CD_3CN) δ(ppm) = -72.40 (d, $^{1}J_{31P\text{-}19F}$ = 707.3 Hz, PF_6^-), -79.08 (s, residue signal, OTf).

^{2}H-NMR (61 MHz, CH_3CN) δ(ppm) = 6.65 (s, -CD_2-).

ESI-MS: m/z [**L-*d*$_8$ PF$_6$** -1PF_6^-]$^+$ calc: 767.12, found: 766.89

Elemental analysis: anal. calc. for $C_{16}H_{20}F_{24}N_8P_4$: C 21.25; H 2.23; N 12.39; S 0.00

found: C 20.35; H 2.53; N 11.47; S 0.18.

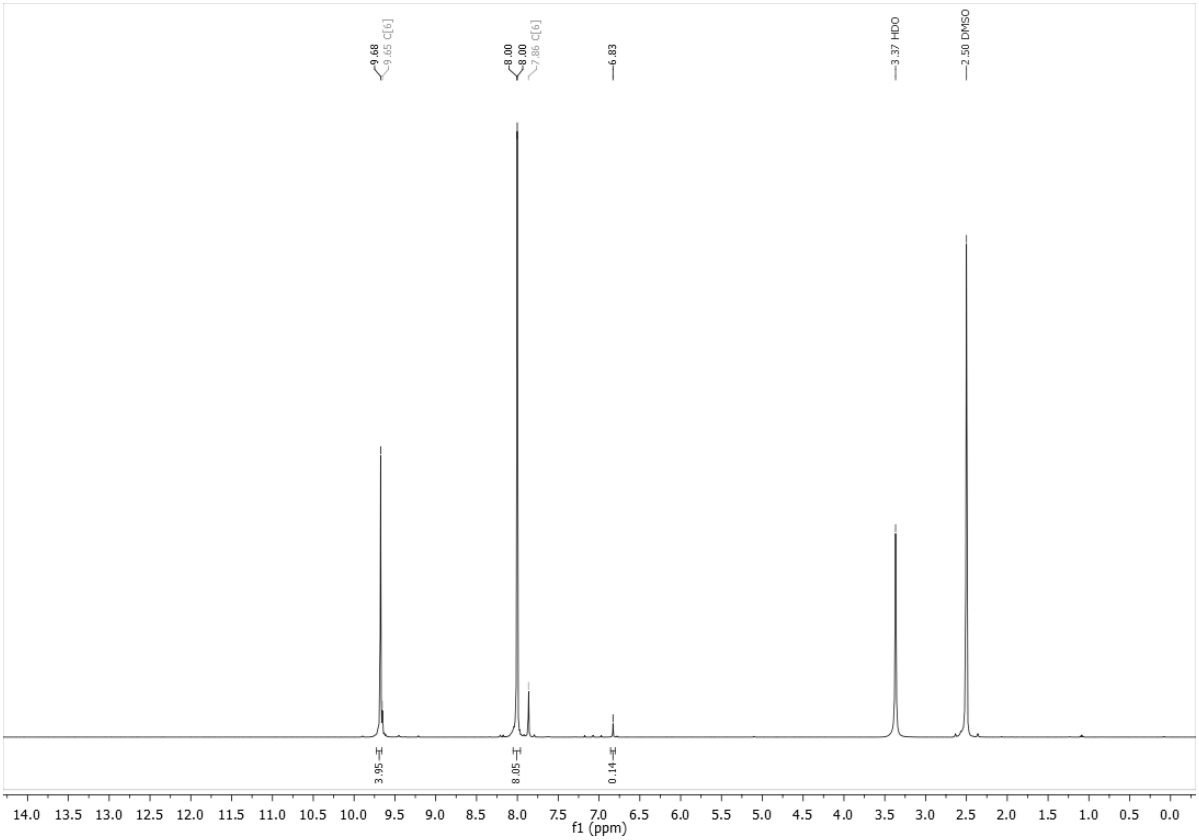

Figure S15. ^{1}H-NMR spectrum of **L-*d*$_8$ PF$_6$** in DMSO-d_6. No loss in deuterium content is visible.

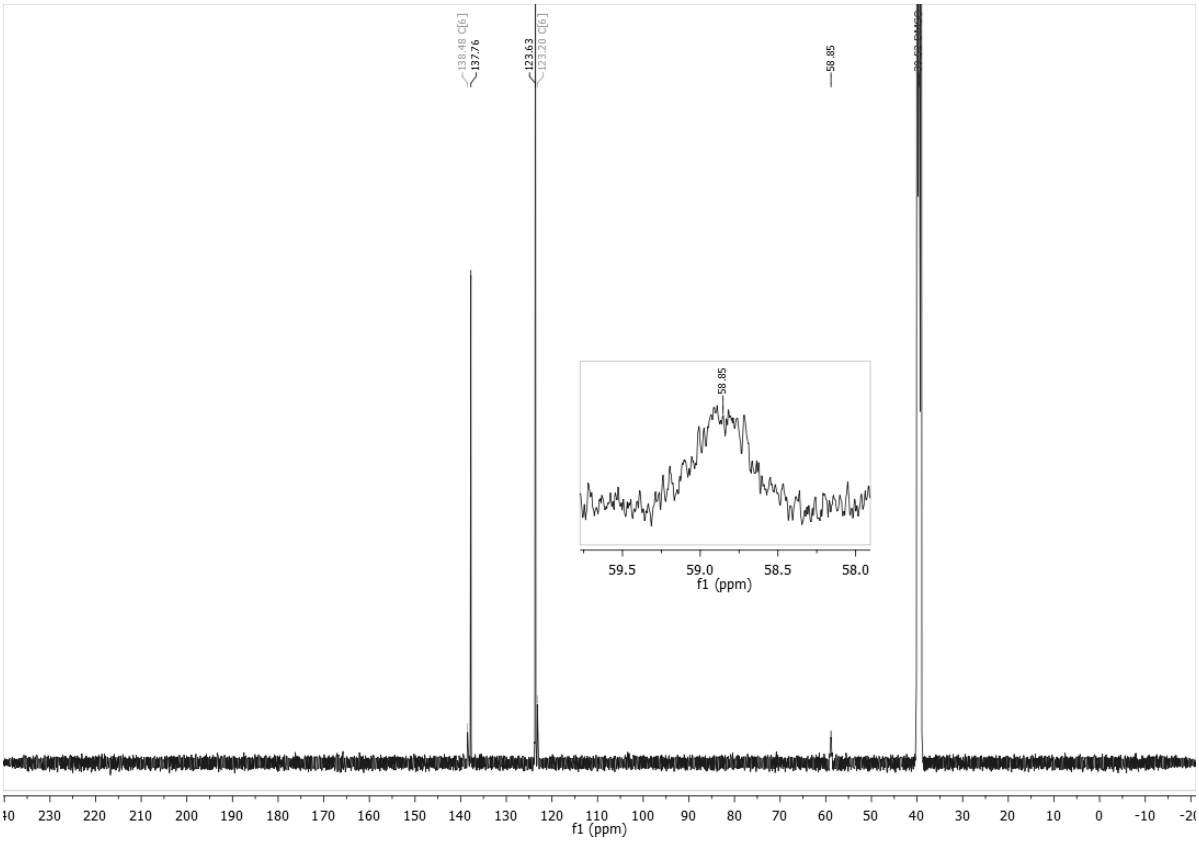

Figure S16. ^{13}C-NMR of **L-*d*$_8$ PF$_6$** in DMSO-*d*$_6$, the multiplet at the methylene bridge (58.85 ppm) is due to $^{1}J_{2H\text{-}13C}$ coupling of the corresponding signal.

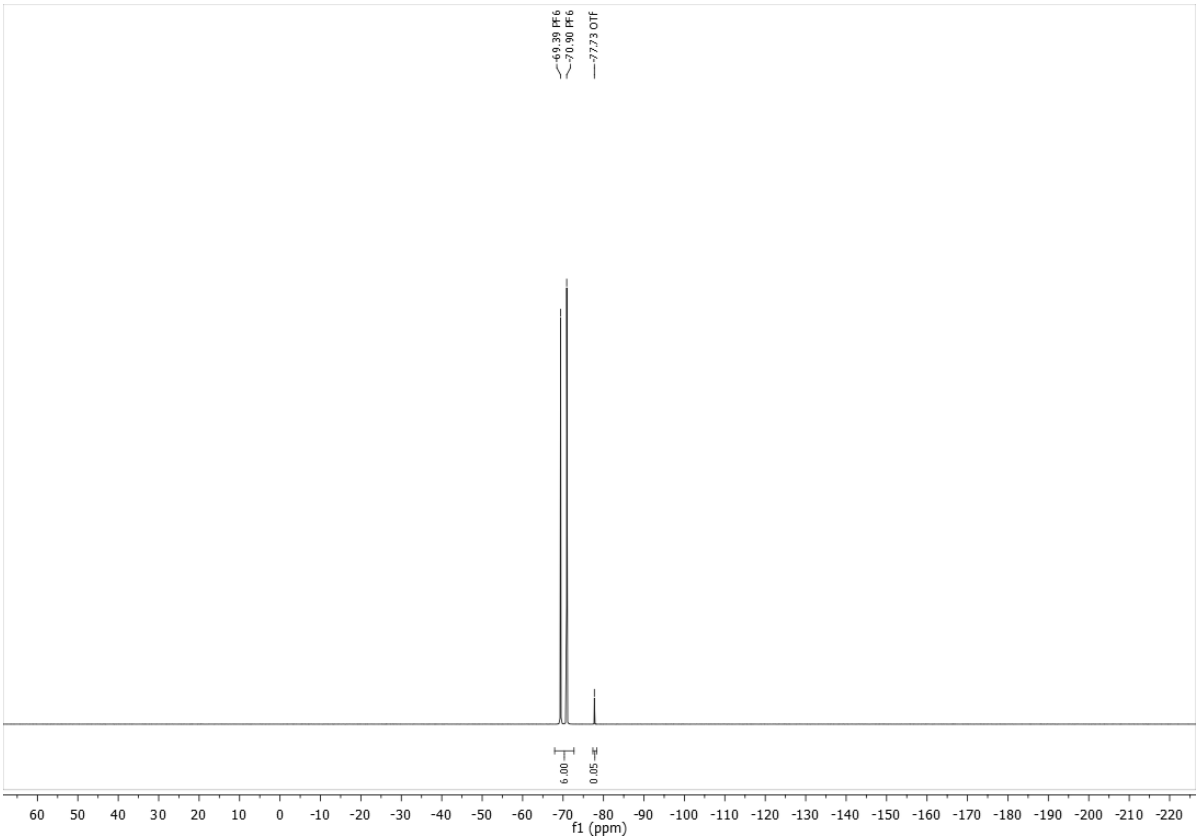

Figure S17. ^{19}F-NMR of **L-*d*$_8$ PF$_6$** in DMSO-*d*$_6$, no reference standard is added, as only the integral ratio is of interest.

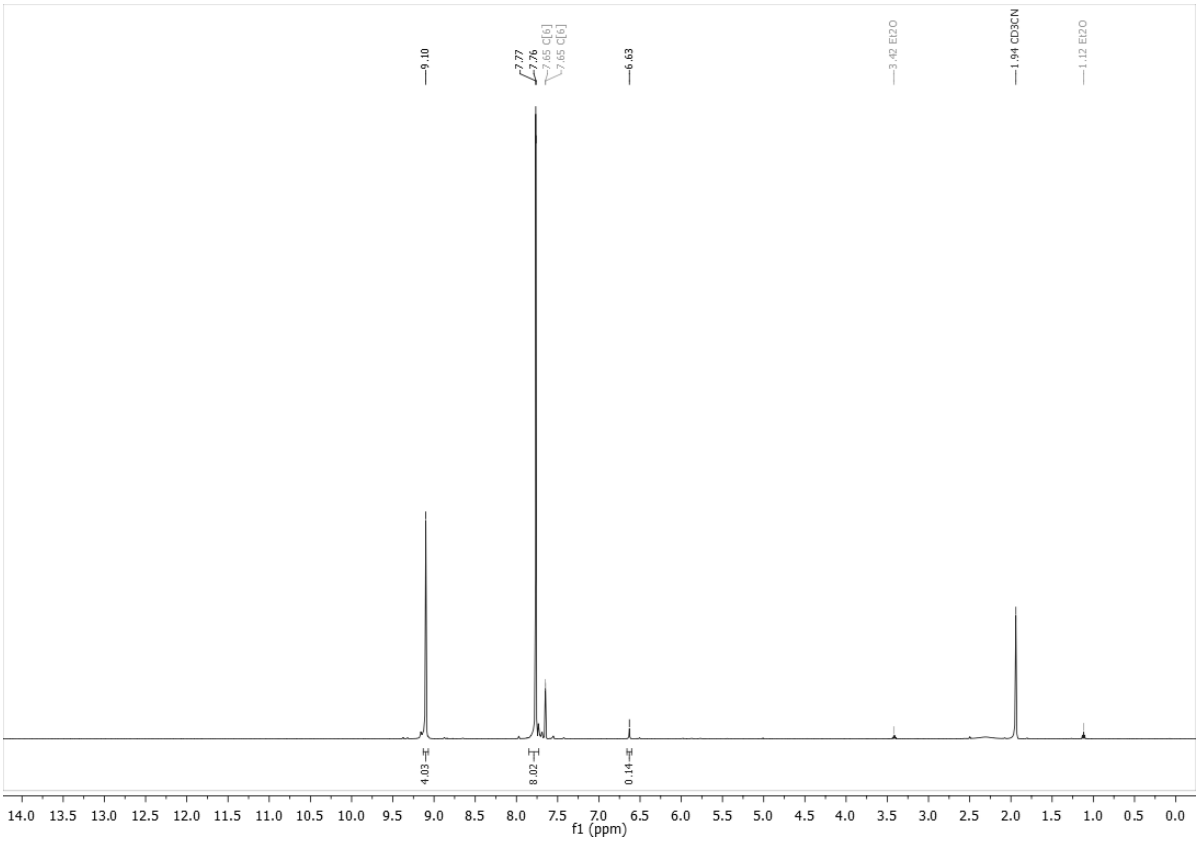

Figure S18. ^{1}H-NMR spectrum of **L-*d*$_8$ PF$_6$** in CD_3CN. No loss in deuterium content is visible.

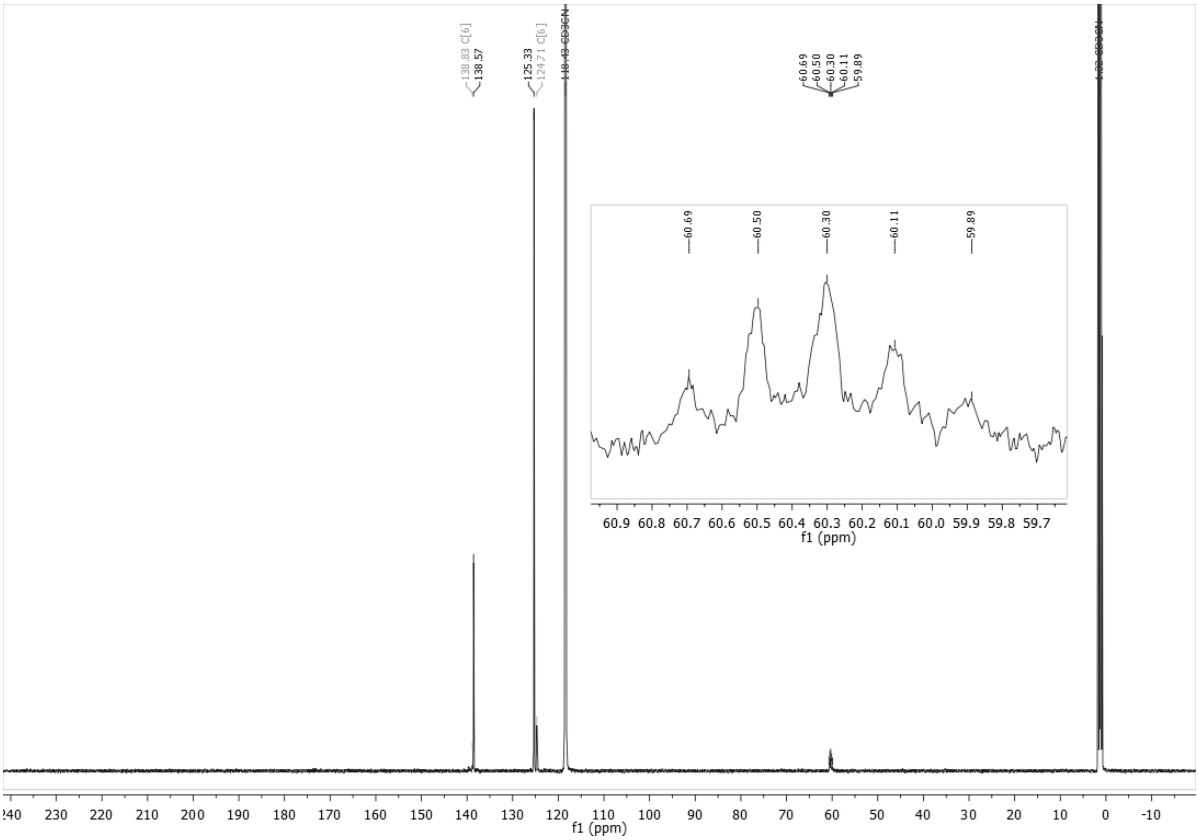

Figure S19. ^{13}C-NMR of **L-*d*$_8$ PF$_6$** in CD_3CN, the methylene bridge (60.30 ppm) shows a triplet of triplet multiplicity due to $^{1}J_{2H\text{-}13C}$ coupling of two deuterium atoms with the ^{13}C at the corresponding location.

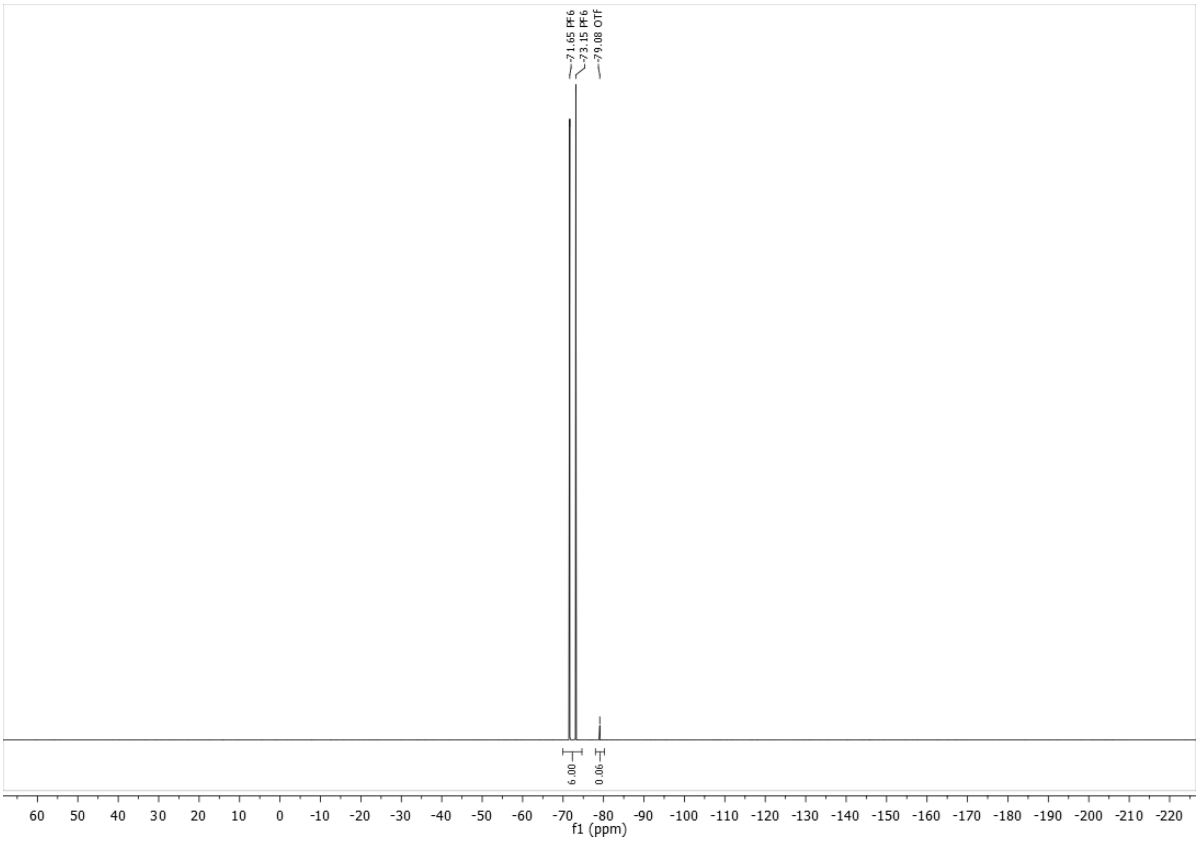

Figure S20. ^{19}F-NMR of **L-*d*$_8$ PF$_6$** in CD_3CN, no reference standard is added, as only the integral ratio is of interest.

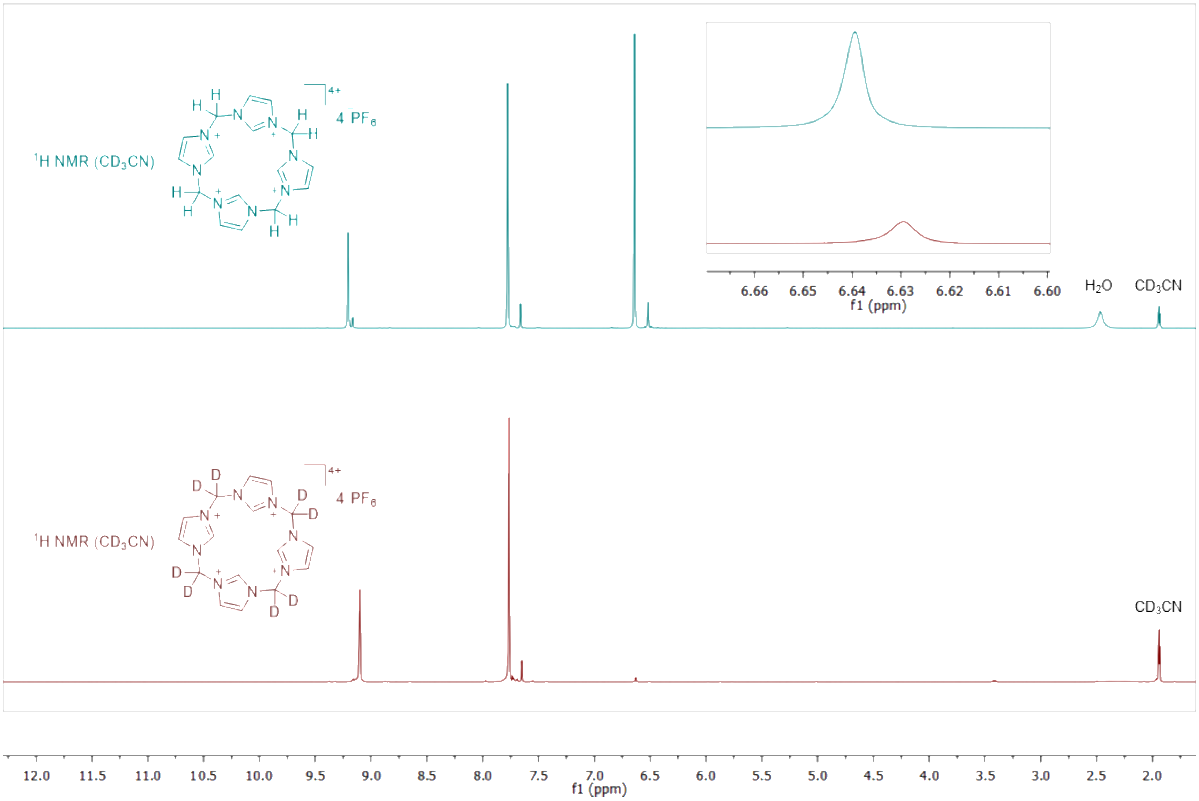

Figure S21. Comparative ^{13}C-NMR spectra of **L-*d*$_8$ PF$_6$** and its non-deuterated analogue, both in CD_3CN.

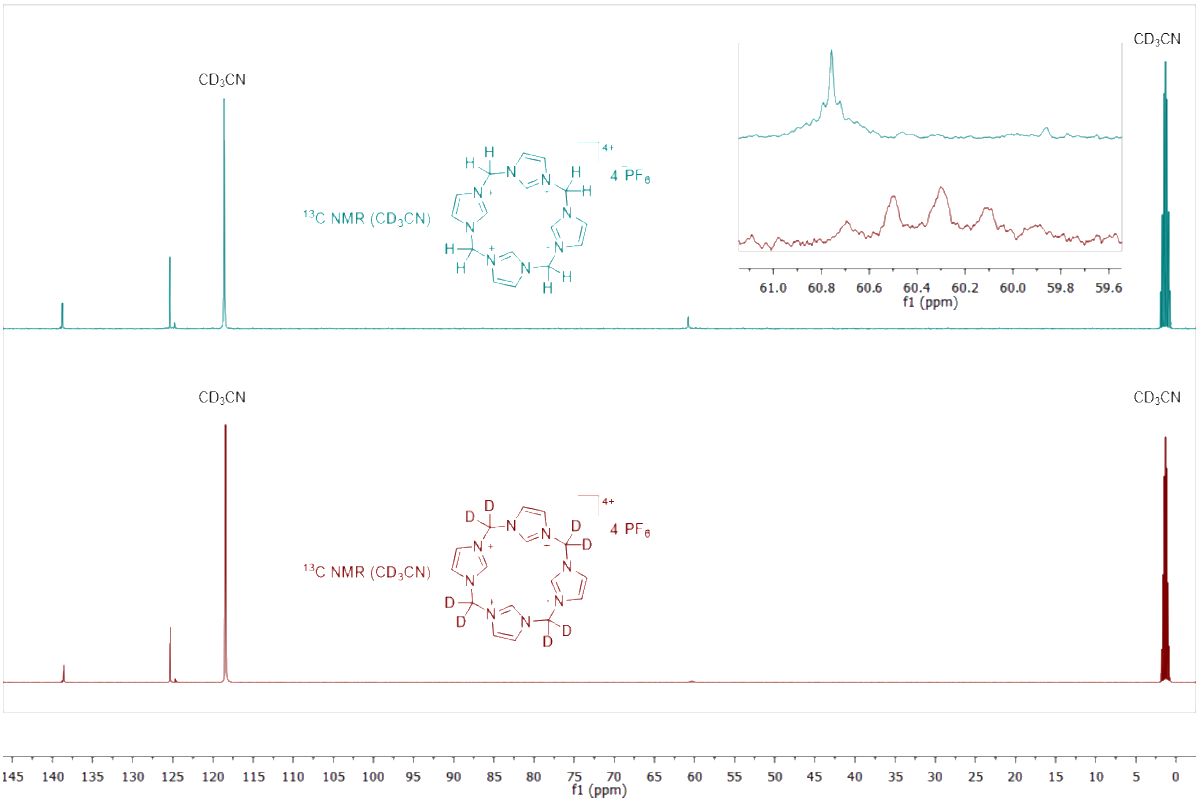

Figure S22. Comparative ^{13}C-NMR spectra of **L-*d*$_8$ PF$_6$** and its non-deuterated analogue, both in CD_3CN.

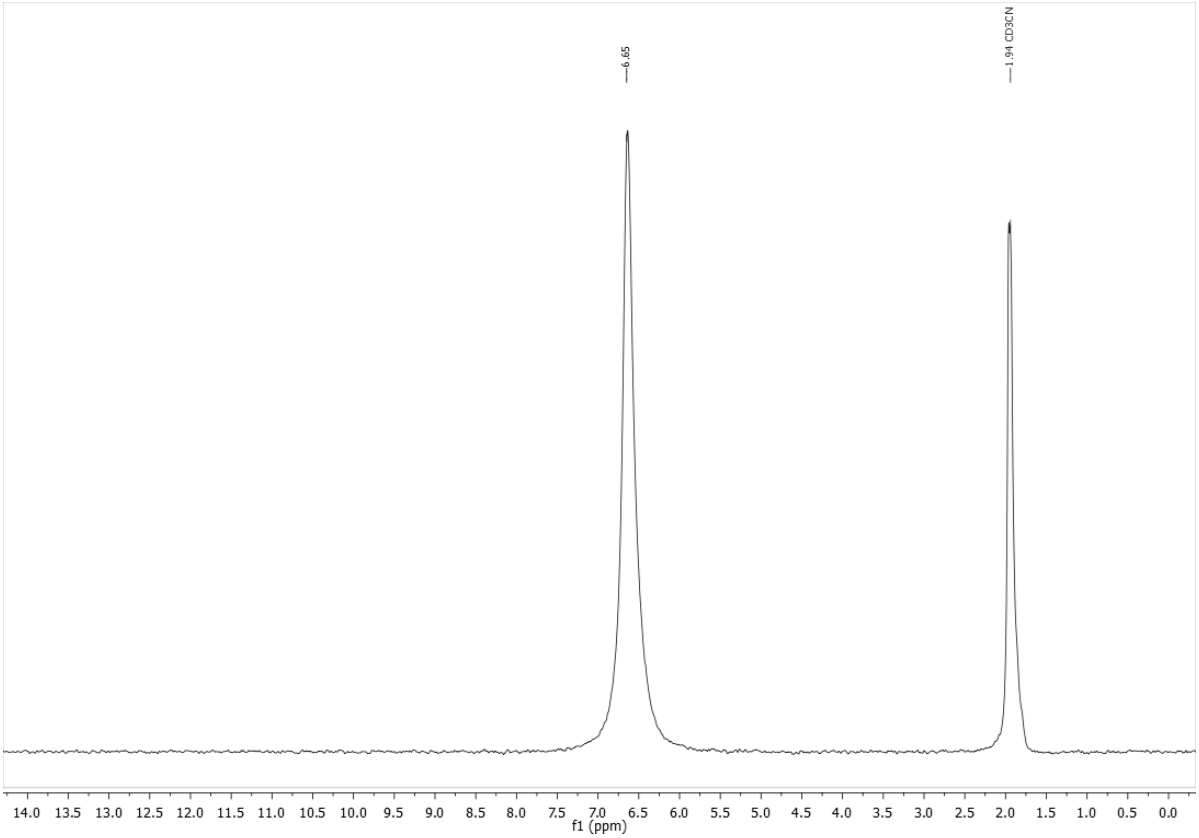

Figure S23. ^{2}H-NMR of **L-*d*$_8$ PF$_6$** in CH_3CN, the chemical shift of the deuterated methylene bridge is in alignment with literature values of a ^{1}H-NMR spectrum for the corresponding chemical environment of a non-deuterated species. CD_3CN is added for referencing.

trans-diacetonitrile[calix[4]imidazoyl-d_8]iron(II) hexafluorophosphate (**1-*d*$_8$**)

The synthesis is performed according to literature procedures utilizing the deuterated ligand **L-*d*$_8$ PF$_6$**. Only dried and degassed solvents are used.[3]

The ^{1}H-NMR spectrum shows the expected signals for the non-deuterated region of the complex and a small signal for the deuterated region, originating from the residual proton content. The ^{2}H-NMR spectrum shows only the signal for the methylene bridge. Here, an equimolar amount of CD_3CN was added towards the sample as internal standard. The deuterium content utilizing the residual proton signal can be determined to be >98%, whereas the ^{2}H-NMR spectrum suggest a deuterium content of the methylene bridges of >95%. No further actions were taken to pinpoint the exact deuterium content, as both values are satisfactorily high.

The ^{13}C-NMR spectrum shows the expected signals for the non-deuterated ligand fragment, the deuterated methylene brigde shows a $^1J_{C\text{-}D}$ coupling, which cannot be resolved. Unexpectedly, the axial coordinating CD_3CN can be resolved and appear as singlet at 129.91 ppm and as unresolvable *ttt* at 3.97 ppm

ESI-MS confirms the success of the synthesis and the presence of the desired deuterium atoms, as the signal corresponds to the signals reported in literature with an increased m/z value of 8 atomic units.

A cyclic voltammetry is performed to ensure that the deuterated iron complexes **1-*d*$_8$** is electronically comparable towards its non-deuterated analogue. The half-cell potential is determined to be $E_{1/2}$ = 0.15 V and is equal to the $E_{1/2}$ of the non-deuterated iron(II) complex.[3]

Fe[N-(SiMe$_3$)$_2$]$_2$(THF) (420.0 mg, 938 µmol, 2.1 eq.) is dissolved in 40 mL acetonitrile and frozen applying liquid nitrogen cooling. On top of that frozen solution, a cooled (-40°C) solution of **L-*d*$_8$ PF$_6$** in 40 mL acetonitrile with a stirring bar is placed. The mixture is allowed to slowly warm to room temperature and stirred for 3 days. The resulting dark solution is reduced to approximately 15 mL volume in *vacuo* and filtered over a short plug of dried silica under argon and is eluated with 120 mL acetonitrile. The solvent is removed *in vacuo* and the residue is re-dissolved in 4.5 mL acetonitrile. Precipitation with 20 mL diethyl ether lead to a yellow solid with brownish contamination. The crude product is washed twice with 0.2 mL acetonitrile and consecutively washed twice with a mixture of 0.2 mL acetonitrile and 2 mL diethyl ether. After a final washing step with diethyl ether and drying *in vacuo* the product is obtained as a yellow solid in 56% yield (185.8 mg, 245.7 µmol).

^{1}H-NMR (400 MHz, CD_3CN) δ(ppm) = 7.59 (s, 8H, N-C*H*-C), 6.30 (s, residual H, -C*D*$_2$-), 1.96 (s, 6H, C*H*$_3$CN).

^{13}C-NMR (126 MHz, CD_3CN) δ(ppm) = 205.26 (N-*C*-N), 129.91 (D_3C-*C*N···Fe), 122.83 (N-*C*H-C), 63.81 – 62.52 (m, $^1J_{2H\text{-}13C}$, -*C*D$_2$-), 4.37 – 3.56 (m, $^1J_{2H\text{-}13C}$, D_3C-CN).

^{2}H-NMR (61 MHz, CH_3CN) δ(ppm) = 6.31 (-*CD*$_2$-).

ESI-MS: m/z [**1-*d*$_8$** -2MeCN -1PF_6^-]$^+$ calc: 529.10, found: 528.82, [**1-*d*$_8$** -2MeCN -2PF_6^- +1$HCOO^-$]$^+$ calc: 429.13, found: 428.92, [**1-*d*$_8$** -2MeCN -2PF_6^-]$^+$ calc: 192.07, found: 192.17

Elemental analysis: anal. calc. for $C_{20}H_{22}F_{12}FeN_{10}P_2$: C 32.10; H 2.96; N 18.72; S 0.00

found: C 31.13; H 2.93; N 17.80; S 0.00.

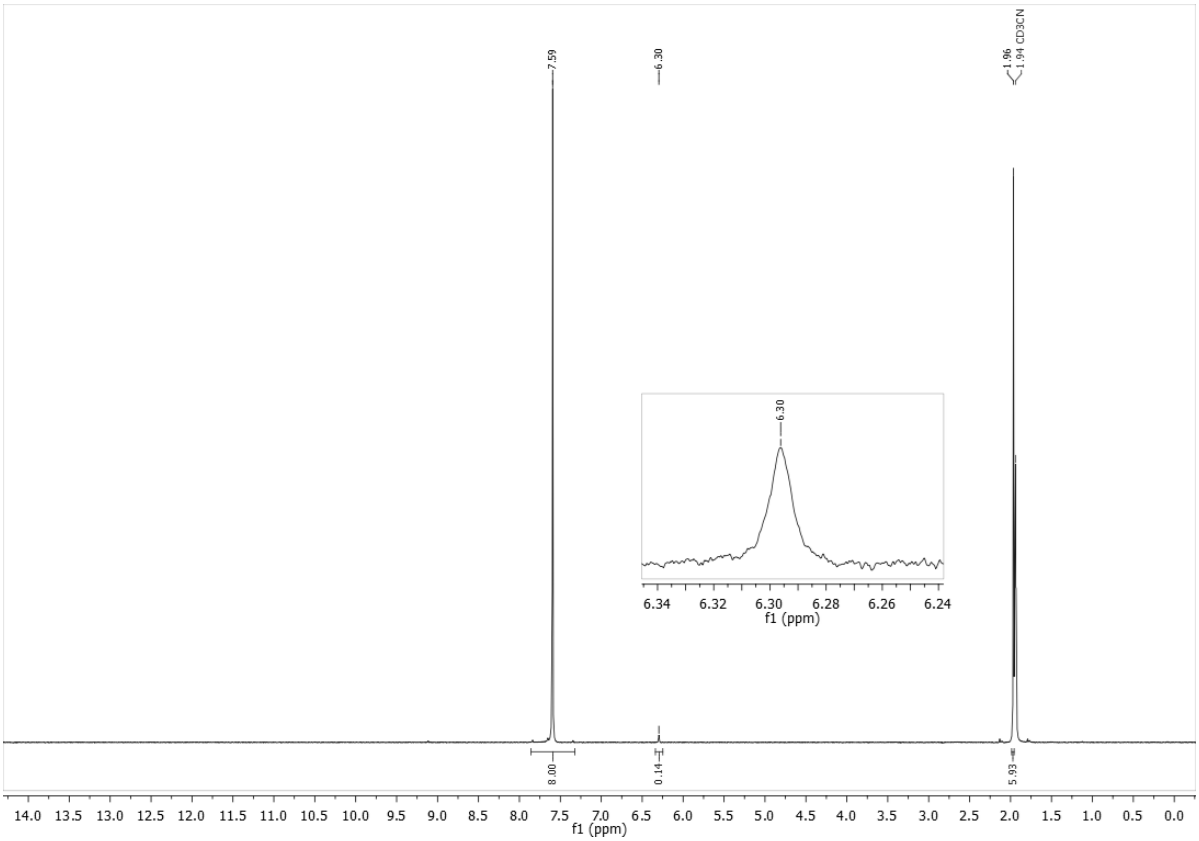

Figure S24. ^{1}H-NMR spectrum of **1-*d*$_8$** in CD_3CN. No loss in deuterium content is visible.

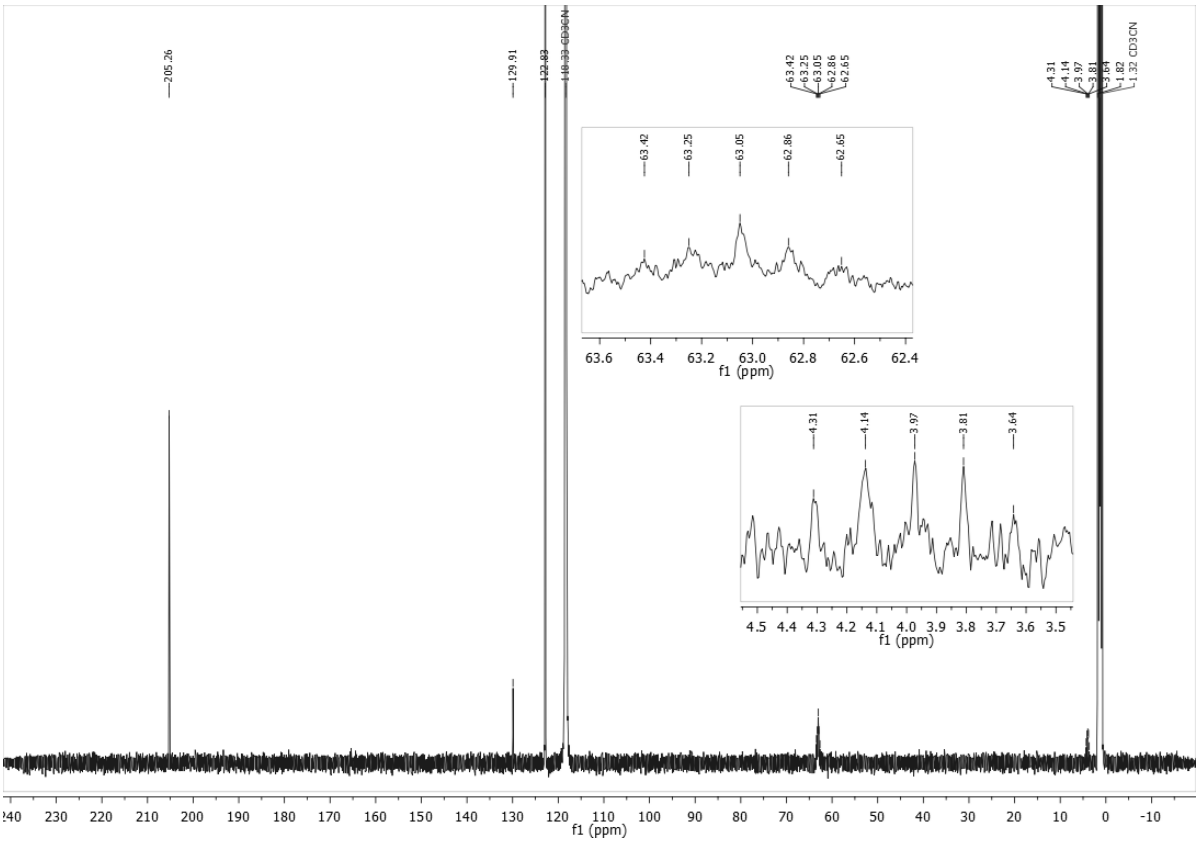

Figure S25. ^{13}C-NMR of **1-*d*$_8$** in CD_3CN, the methylene bridge (63.05 ppm) still shows a triplet of triplet multiplicity due to $^{1}J_{2H\text{-}13C}$ coupling of two deuterium atoms with the ^{13}C at the corresponding location, but cannot be resolved fully. Interestingly, signals for the coordinating acetonitrile are found at 129.91 and 3.97 ppm. The multiplet at 3.97 ppm, which should be a ttt but cannot be resolved completely, suggests that deuterated acetonitrile is coordinating axially.

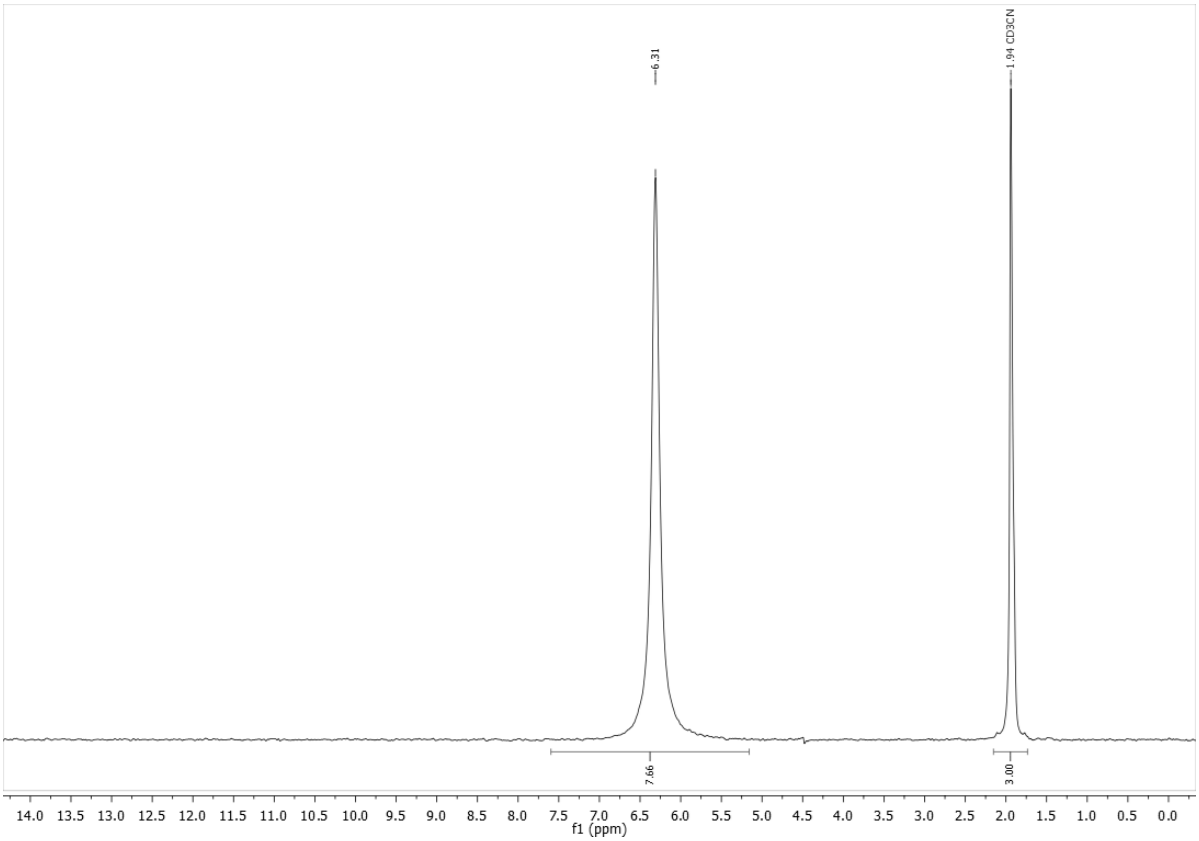

Figure S26. ^{2}H-NMR spectrum of **1-*d*$_8$** in CH_3CN, the chemical shift of the deuterated methylene bridge is in alignment with literature values of a ^{1}H-NMR spectrum for the corresponding chemical environment of a non-deuterated species. An equimolar amount of CD_3CN was added to the sample as internal standard.

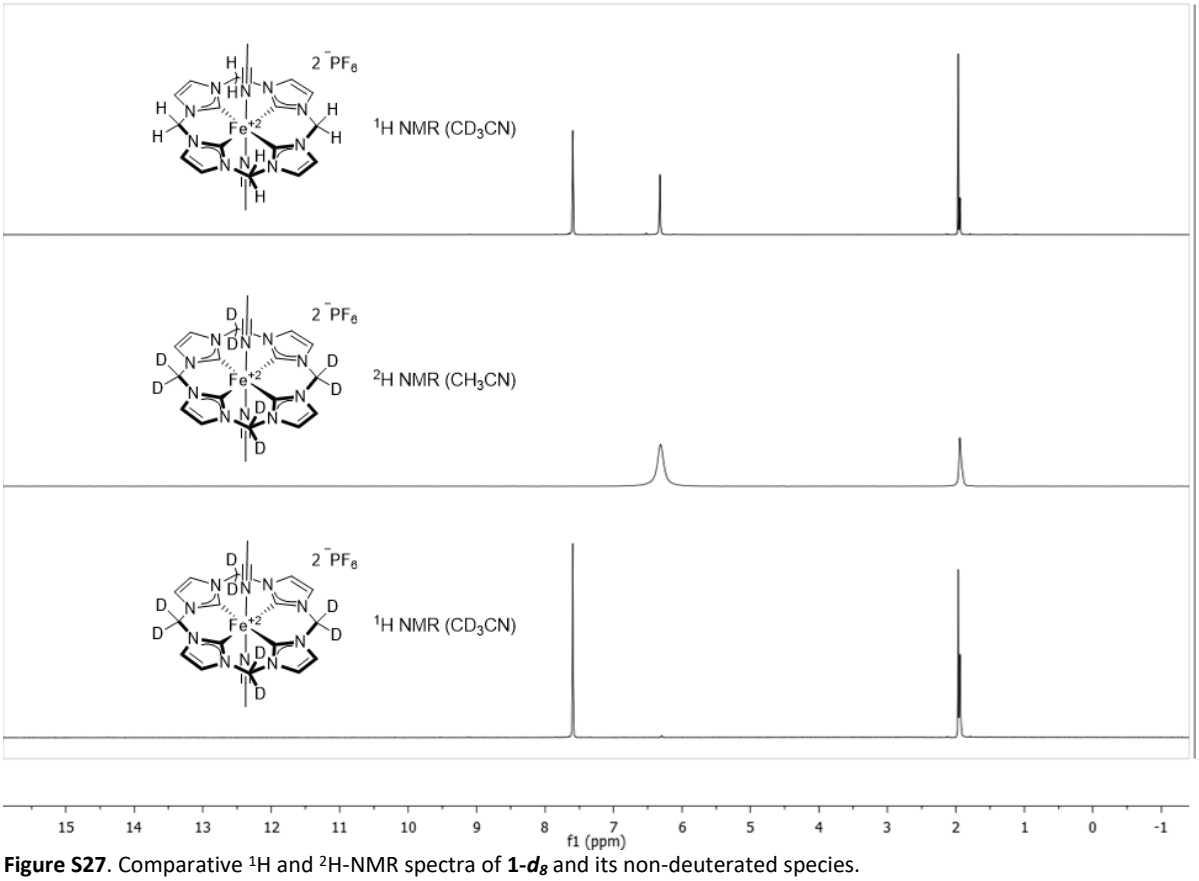

Figure S27. Comparative ^{1}H and ^{2}H-NMR spectra of **1-*d*$_8$** and its non-deuterated species.

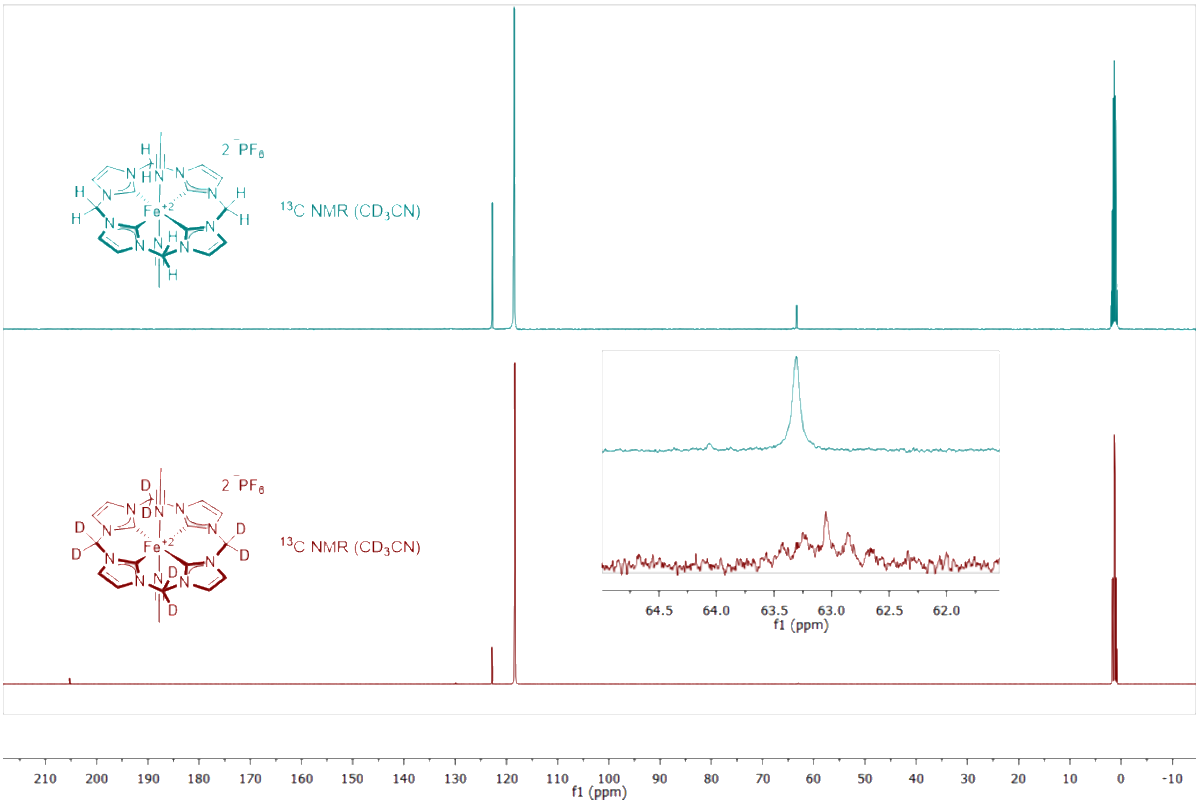

Figure S28. Comparative ^{13}C-NMR spectra of **1-*d*$_8$** and deuterated species. The carbene signal in the non-deuterated analogue could not be resolved.

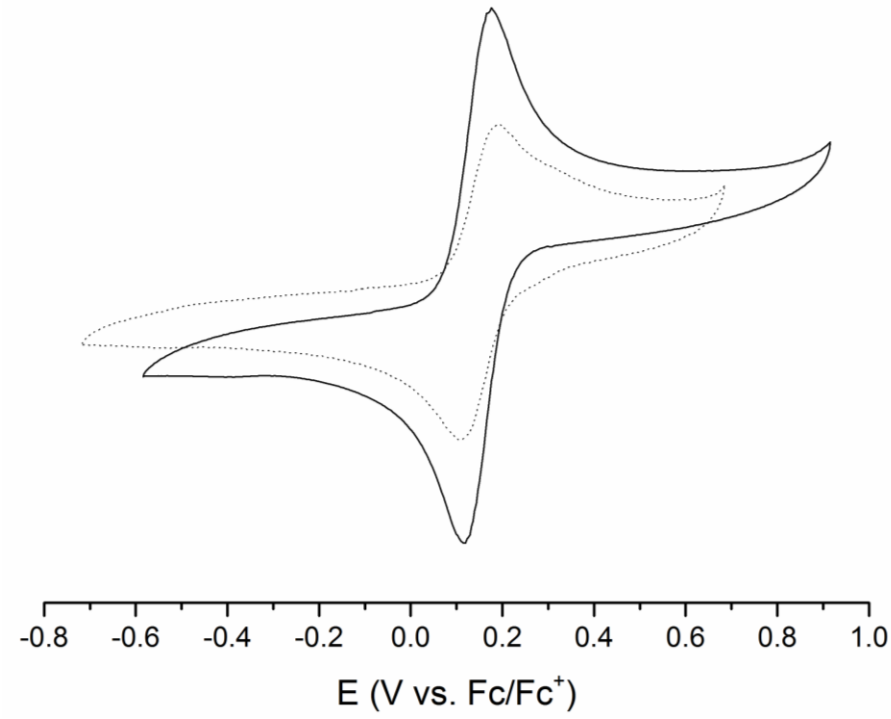

Figure S29. Cyclic voltammogram of complex **1-*d*$_8$** (solid line) in comparison to complex **1** (dotted line). The half-cell potential of **1-*d*$_8$** is determined to be $E_{1/2}$ = 0.15 V, with an oxidation potential $E_{ox.}$ = 0.18 V and a reduction potential $E_{red.}$ = 0.12 V, referenced to the half-cell potential of the Fc/Fc$^+$ redox couple. These values are in alignment with the reported values of complex **1**.[3]

trans-diacetonitrile[calix[4]imidazoyl-*d*$_8$]iron(III) hexafluorophosphate (**2-*d*$_8$**)

The synthesis is performed according to literature procedures utilizing the deuterated complex **1-*d*$_8$**. Only dried and degassed solvents are used.[7]

The ^{2}H-NMR spectrum shows one paramagnetic shift at 43.60 ppm for the deuterated methylene bridge. This signal can be seen, slightly shifted, in the ^{1}H-NMR spectrum at 44.54 ppm as residual proton signal. Here, the signal for the backbone protons are present at 108.69 ppm. ESI-MS shows multiple signals for the cationic complex fragment with different anion combinations.

1-*d*$_8$ (103.5 mg, 136.8 µmol, 1.0 eq.) is dissolved in 12 mL acetonitrile and cooled to -40 °C. Thianthrenyl hexafluorophosphate (58.3 mg, 161.4 µmol, 1.15 eq.) dissolved in 11 mL acetonitrile is added. The mixture is allowed to warm to room temperature and stirred for 1 h. The resulting violet solution is reduced to 5 mL volume and precipitated upon addition of 70 mL diethyl ether. The filtered solid is washed twice with a mixture of 1 mL acetonitrile and 4 mL diethyl ether and consecutively washed twice with 3 mL diethyl ether. After drying *in vacuo* the product is obtained as violet solid in 84% yield (103.7 mg, 115.0 µmol)

Due to the paramagnetic nature of this compound the deuterium content cannot reliably determined *via* ^{1}H-NMR spectroscopy. The deuterated species is the primary species found in HR-MS.

^{1}H-NMR (400 MHz, CD_3CN) δ(ppm) = 108.69 (s, N-C*H*-CH), 44.54 (s, residual H, -C*D*$_2$-).

^{2}H-NMR (61 MHz, CH_3CN) δ(ppm) = 43.60 (s, -C*D*$_2$-).

ESI-MS: m/z [**2-*d*$_8$** -3PF_6^- -2MeCN+$HCOO^-$]$^{2+}$ calc: 214.57, found: 214.54; [**2-*d*$_8$** -3PF_6^- -2MeCN +F^-+$HCOO^-$]$^+$ calc: 448.13, found: 448.07; [**2-*d*$_8$** -2PF_6^- -2MeCN + F^-]$^+$ calc: 548.10, found: 547.81; [**2-*d*$_8$** -2PF_6^- -2MeCN+ $HCOO^-$]$^+$ calc: 574.10, found: 573.62; [**2-*d*$_8$** -1PF_6^- -1MeCN]$^+$ calc: 715.09, found: 715.64

Elemental analysis: anal. calc. for $C_{20}H_{14}D_8F_{18}FeN_{10}P_3$: C 26.89; H 2.48; N 15.68; S 0.00
found: C 27.72; H 2.69; N 15.25; S 0.00.

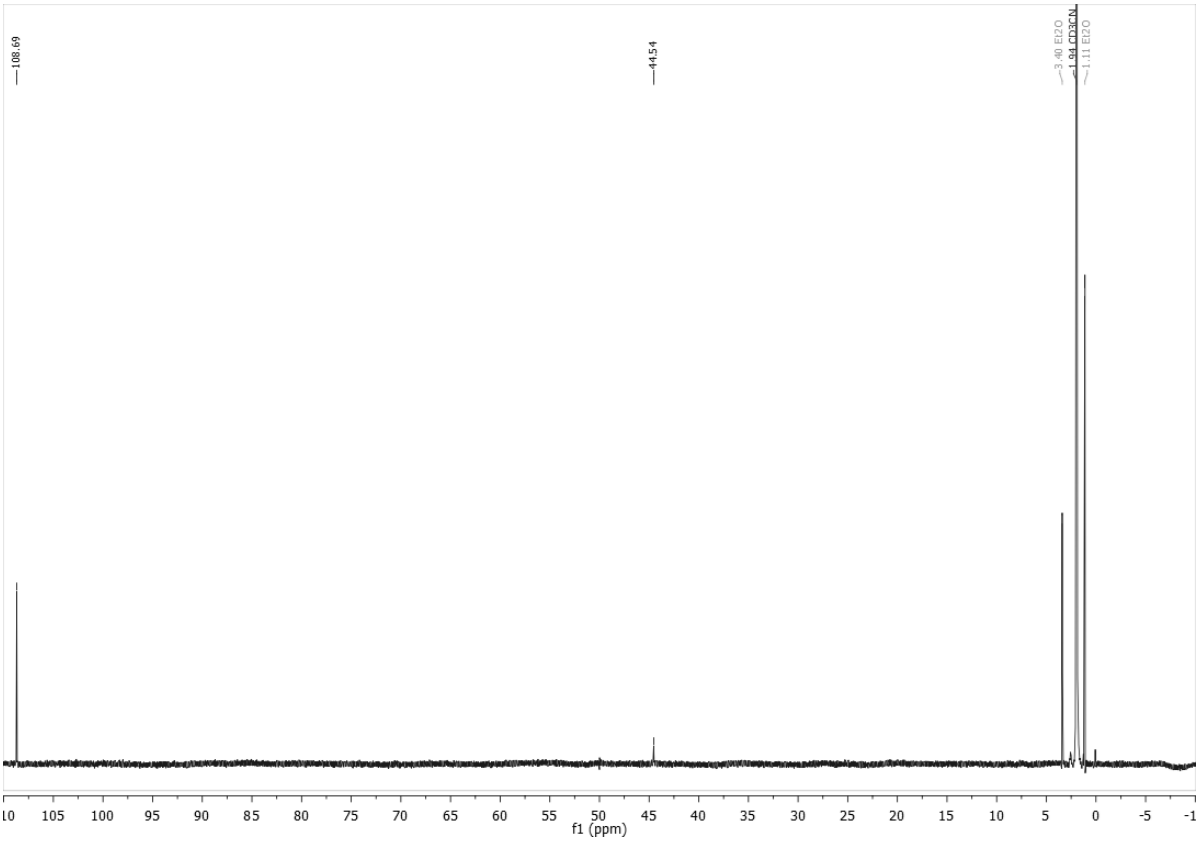

Figure S30. Paramagnetic ^{1}H-NMR spectrum of **2-*d*$_8$** in CD_3CN. Signal integration was not performed due to the paramagnetic nature of the signals.

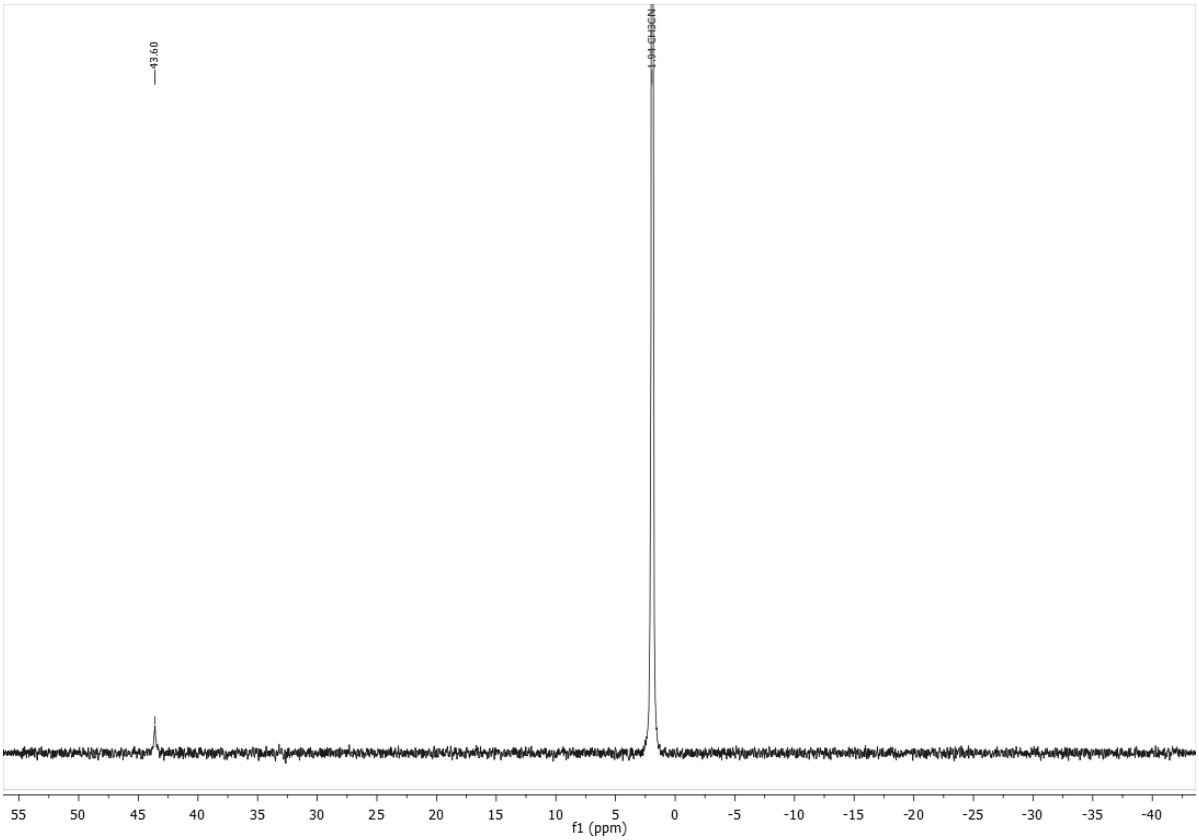

Figure S31. ^{2}H-NMR spectrum of **2-*d*$_8$** in CH_3CN, CD_3CN is added as referencing standard.

4. ESI-MS Decomposition Studies

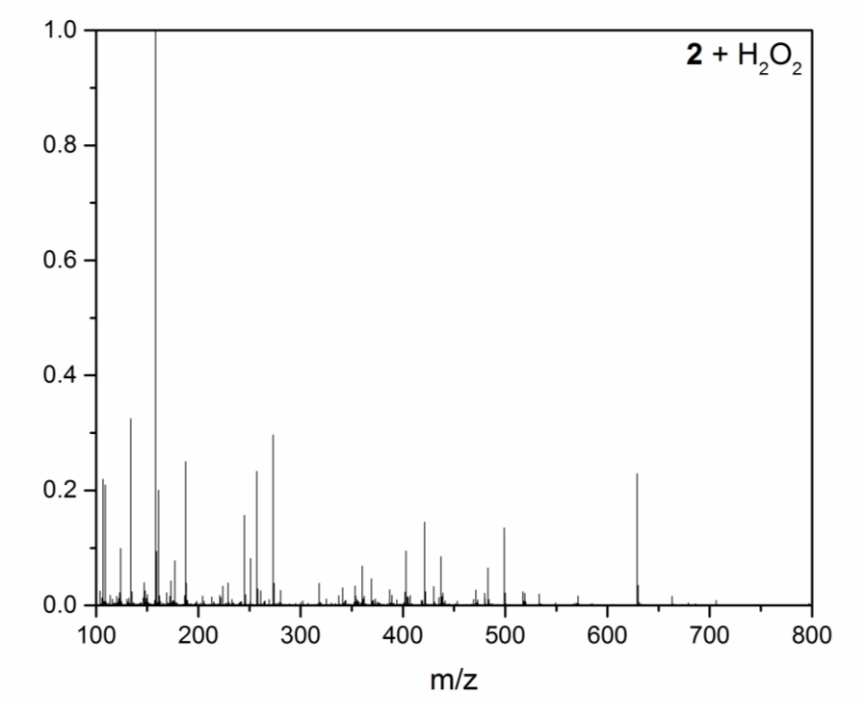

Figure S32. HR-ESI-MS spectrum obtained immediately after addition of 10 eq. H_2O_2 (50% in water) to a solution of **2** (c = 0.1 mg/mL) in MeCN.

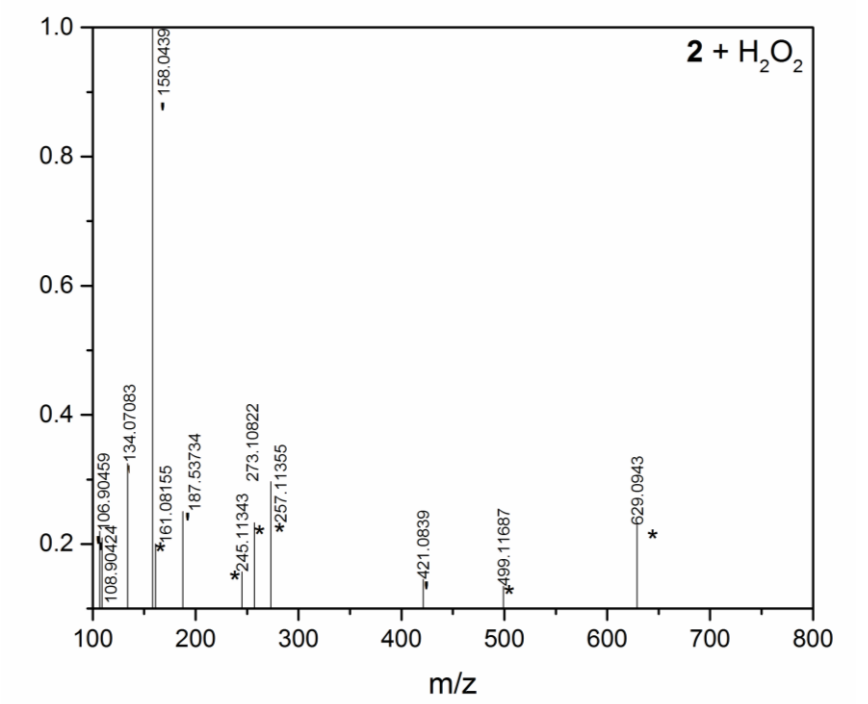

Figure S33. HR-ESI-MS spectrum acquired 15 s after addition of 10 eq. H_2O_2 (50% in water) to a solution of **2** (c = 0.1 mg/mL) in MeCN (relative intensity >10%). Signals of **5** are observed (marked with *, see Figures S36 and S37 for reference spectra). In addition, m/z values assignable to a species featuring Fe^{III}, two MeCN ligands and one mono-oxidised unprotonated macrocyclic NHC ligand (marked with ‘) are observed (for detailed comparison of main peak m/z = 158.0439 with theoretical isotope pattern see Figure S35). DFT calculations rationalize the theoretical existence of such a compound (SI, chapter 5), which presumably represents an intermediate in the formation of **5**.

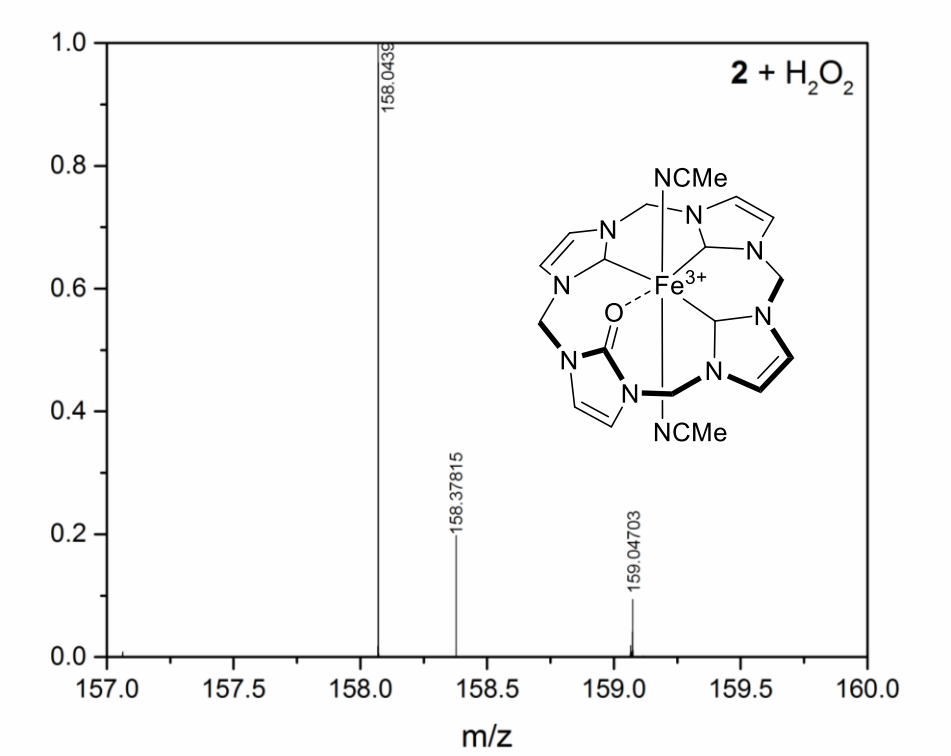

Figure S34. Section of the HR-ESI-MS spectrum acquired 15 s after addition of 10 eq. H_2O_2 (50% in water) to a solution of **2** (c = 0.1 mg/mL) in MeCN, showcasing the measured isotope distribution of Fe^{III} species with two MeCN ligands and one mono-oxidised unprotonated macrocyclic NHC ligand corresponding to a chemical formula of $[C_{20}H_{22}FeN_{10}O]^{3+}$.

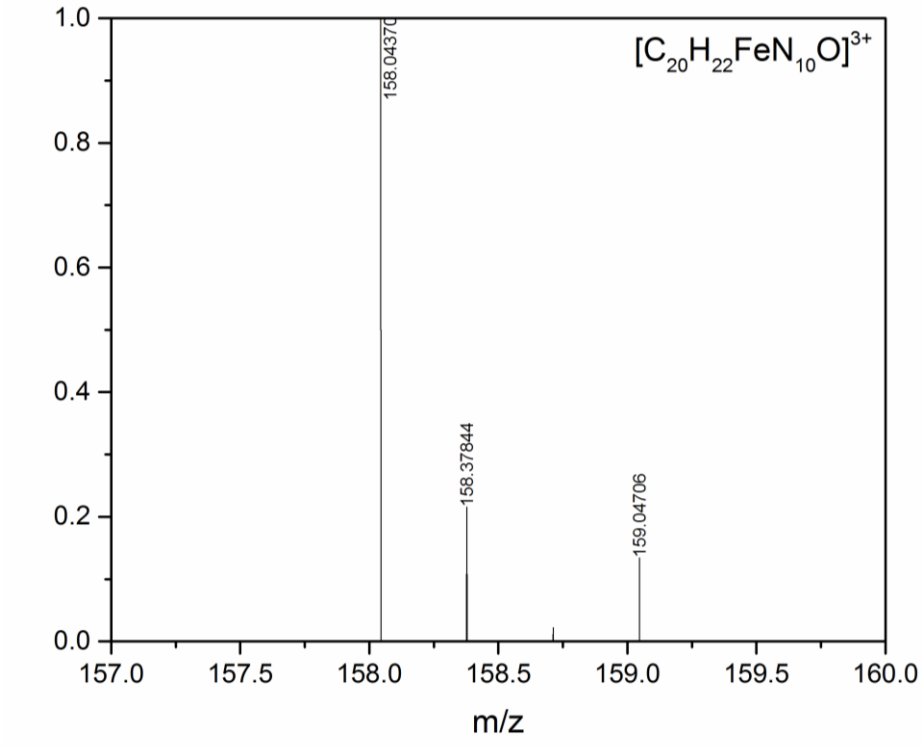

Figure S35. Calculated isotope pattern of $[C_{20}H_{22}FeN_{10}O]^{3+}$.

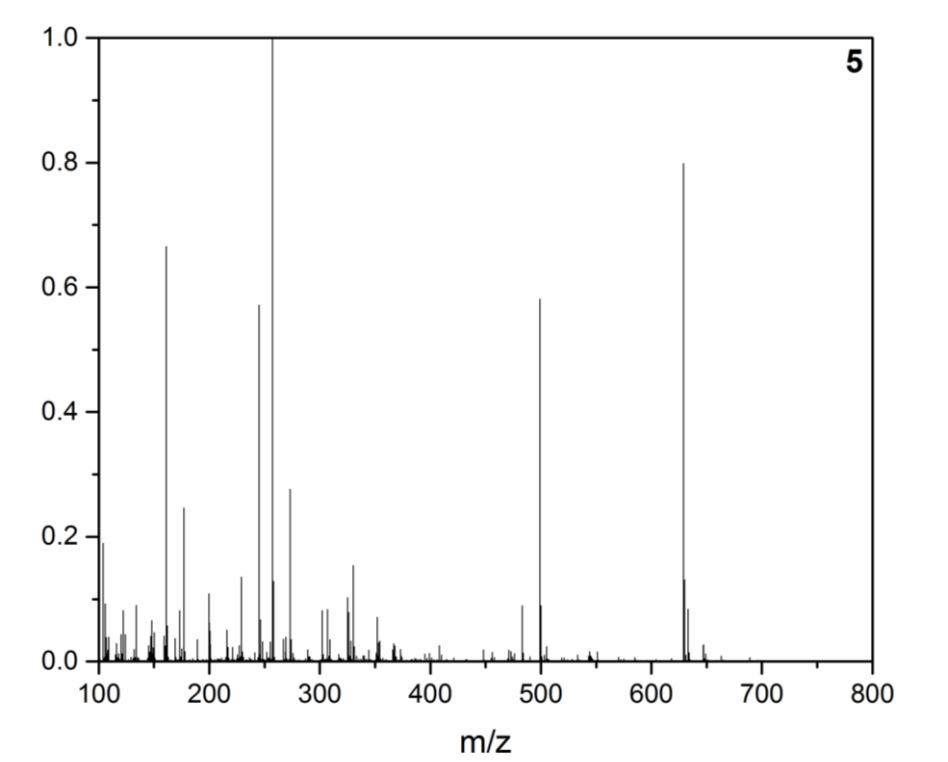

Figure S36. HR-ESI-MS spectrum of **5**.

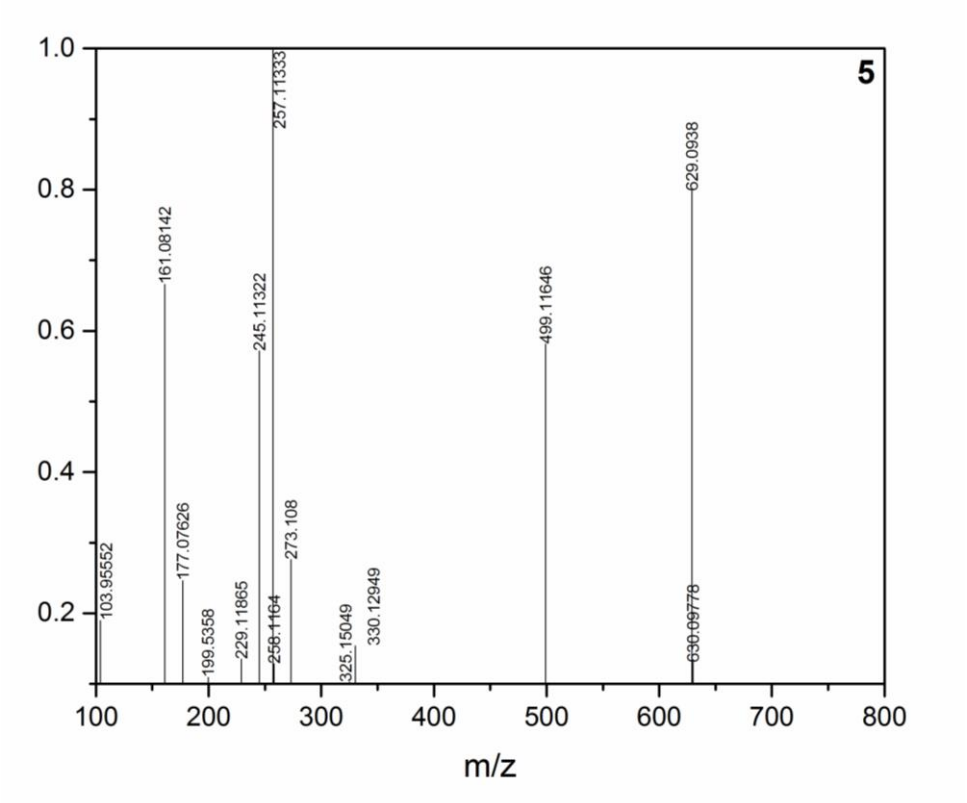

Figure S37. HR-ESI-MS spectrum of **5** (relative intensity >10%).

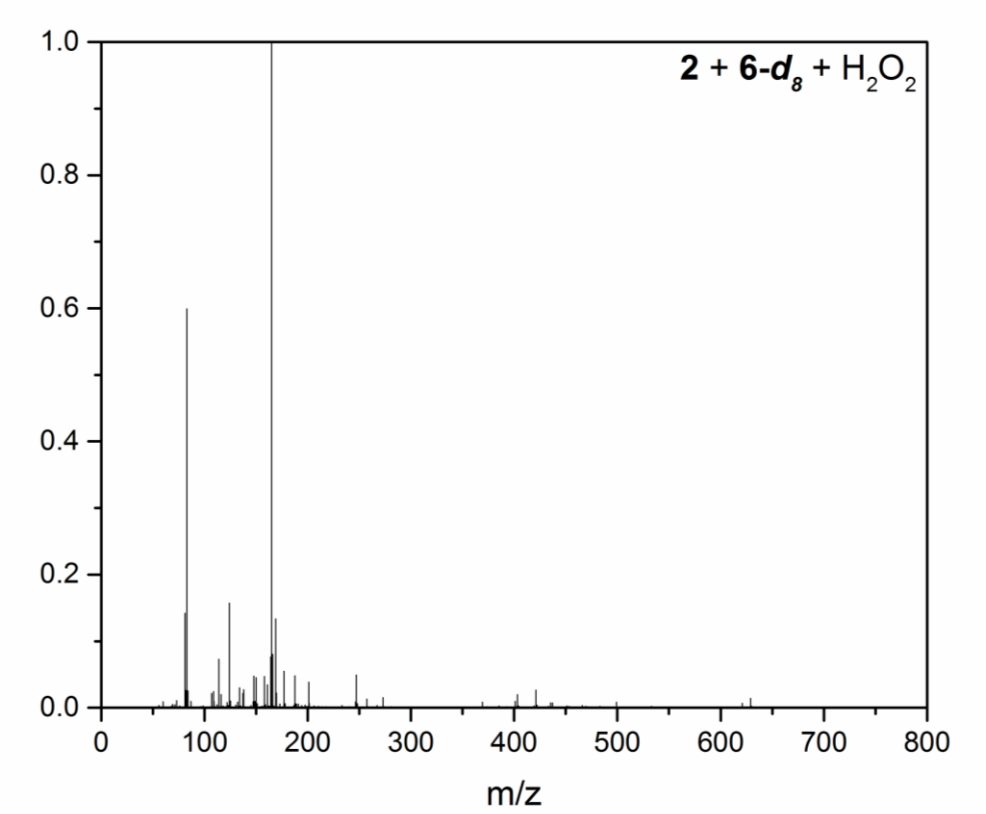

Figure S38. Full HR-ESI-MS spectrum obtained after addition of 5 eq. **6-*d*$_8$**, followed by 10 eq. H_2O_2 to a solution of **2** in MeCN.

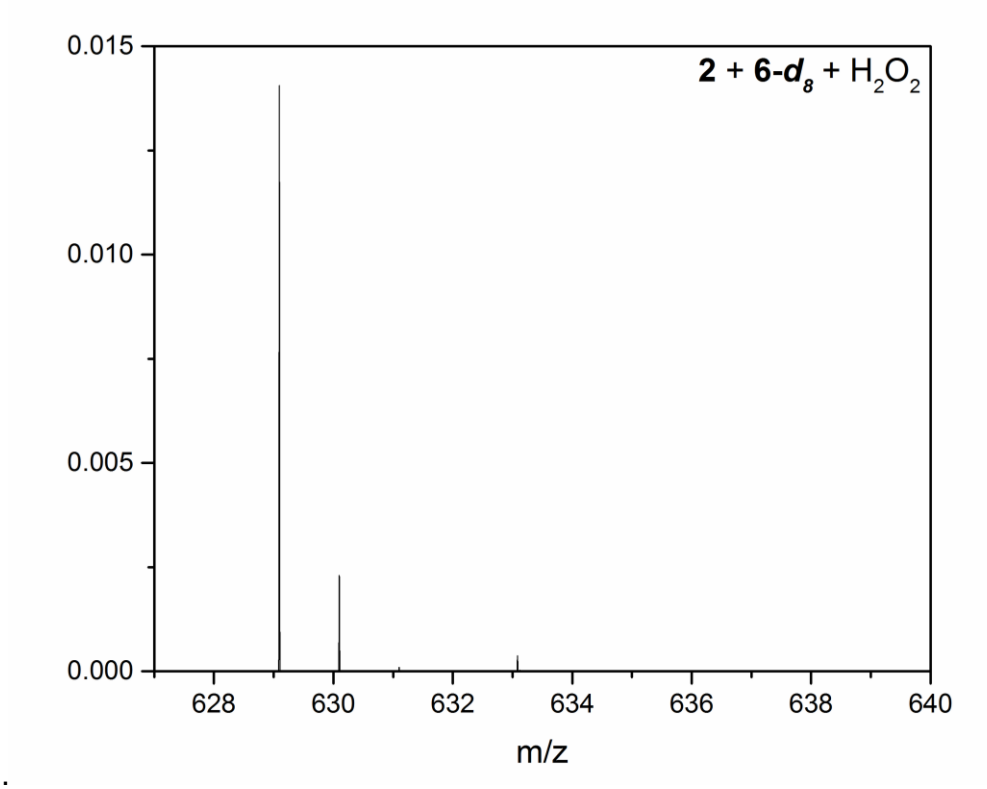

.

Figure S39. Section of the HR-ESI-MS spectrum obtained after addition of 5 eq. **6-*d*$_8$**, followed by 10 eq. H_2O_2 to a solution of **2** in MeCN. If oxidation of the ligand would occur after protonation, a signal with a m/z value of 637.15 corresponding to the formula $C_{16}H_{11}D_8F_{12}N_8OP_2^+$ should be visible. Instead, only the respective signal of undeuterated compound **5** corresponding to the formula $C_{16}H_{19}F_{12}N_8OP_2^+$ is observed (m/z = 629.10). In conjunction with the observation, that an Fe^{III} species with oxidised and unprotonated ligand was observed previously (Figure S33), the protonation of the ligand presumably occurs after its oxidation.

5. DFT Calculations

Two ground state structures are obtained with either a *cis*- or a *trans*-configuration of the respective acetonitrile ligands. Both electronic structures are feasible with a HOMO-LUMO gap of 7.6 eV (*cis*) and 7.9 eV (*trans*). The trans configuration is energetically favored by 8.4 kJ/mol (Gibbs free energy) and corresponds highly likely to the oxidised Fe^{III} complex observed in ESI-MS experiments (Figure S32-S34).

All calculations are performed using Orca 4.2.1[8] built with the libXC program 4.2.3[9]. Visualisation and processing is performed in ChemCraft. The libint2 library is used for the computation of 2-electron integrals.[10] Quasirelativistic calculations (ZORA with one-center approximation) are performed using the wb97x functional[11] with the D30 dispersion correction[12]. Light atoms are treated with the ZORA-def2-SVP basis set and Fe with ZORA-def2-TZVP.[13] In order to speed up calculations, the RIJCOSX approximation is used in combination with a gridx of 4 and the auxiliary basis SARC/J.[14] Numerical precision was ensured by using grid 6 for all atoms, an integration accuracy of 6 for light atoms and an increased integration accuracy of 10 for Fe. Final grid is suppressed using the keywords nofinalgrid. Convergence criteria for the SCF and the optimisation are set to tight. The obtained structures are true ground states as shown by the absence of significant imaginary frequencies (< 12 cm^{-1}).

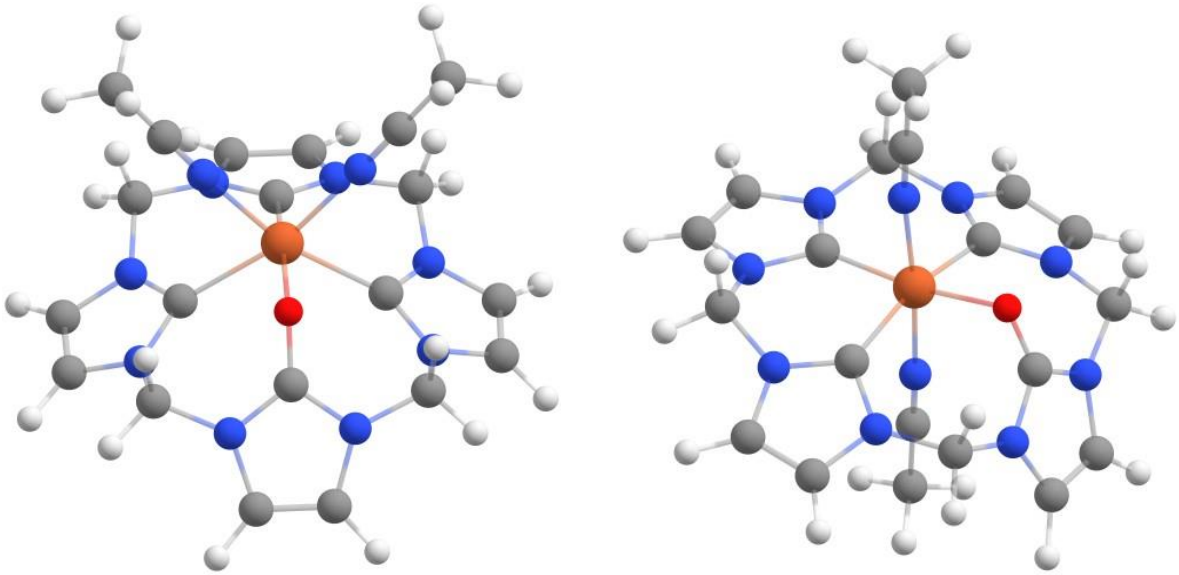

Figure S40. Feasible ground state structures of the intermediary $[C_{20}H_{22}FeN_{10}O]^{3+}$ species in *cis*- (left) and *trans*-configuration (right) obtained in optimisation calculations using DFT.

Table S2. XYZ-coordinates for the *cis*-$[C_{20}H_{22}FeN_{10}O]^{3+}$ species (charge 3, multiplicity 2, G° = -2677.89614 h)

8	-0.003874000	-1.508332000	1.200155000
7	1.076763000	-3.156034000	-0.043318000
7	-1.075908000	-3.157690000	-0.049104000
7	-2.519285000	-1.333212000	-0.619890000
7	-2.565915000	0.728019000	-1.149649000
7	-1.061059000	2.554739000	-1.259443000
7	1.053327000	2.553463000	-1.263754000
7	2.562913000	0.729396000	-1.147446000
7	2.519655000	-1.329833000	-0.610512000

6	-0.001366000	-2.531196000	0.455042000
6	0.676047000	-4.183981000	-0.901332000
1	1.383827000	-4.839860000	-1.387713000
6	-0.669132000	-4.185077000	-0.904834000
1	-1.373461000	-4.841999000	-1.394841000
6	-2.362857000	-2.575060000	0.145570000
1	-2.496903000	-2.357421000	1.206917000
1	-3.134727000	-3.271908000	-0.177868000
6	-1.770955000	-0.195177000	-0.555413000
6	-3.720717000	-1.114518000	-1.278536000
1	-4.435999000	-1.905702000	-1.453916000
6	-3.754184000	0.185757000	-1.608892000
1	-4.499846000	0.769226000	-2.130465000
6	-2.422708000	2.164800000	-1.020256000
1	-2.731116000	2.472749000	-0.017759000
1	-3.064962000	2.649789000	-1.755222000
6	-0.003185000	1.913004000	-0.732514000
6	-0.679235000	3.585166000	-2.097028000
1	-1.390220000	4.217461000	-2.610093000
6	0.669315000	3.584557000	-2.099496000
1	1.379026000	4.216293000	-2.615024000
6	2.415994000	2.166642000	-1.024769000
1	3.056386000	2.649548000	-1.762759000
1	2.725091000	2.479785000	-0.024031000
6	1.768150000	-0.193694000	-0.552880000
6	3.755103000	0.188723000	-1.598912000
1	4.501228000	0.772169000	-2.119840000
6	3.723486000	-1.110456000	-1.264473000
1	4.441140000	-1.900652000	-1.434604000
6	2.361521000	-2.570470000	0.156835000
1	3.136334000	-3.266540000	-0.161225000
1	2.489528000	-2.350635000	1.218460000
26	-0.002573000	0.304110000	0.429674000
7	1.347652000	0.932432000	1.775875000
6	2.018908000	1.179400000	2.672299000
6	2.860982000	1.484490000	3.813453000
1	2.607392000	2.473035000	4.205359000
1	2.697900000	0.735261000	4.593154000
1	3.913016000	1.471348000	3.517580000
6	-2.016514000	1.189003000	2.676413000
6	-2.850833000	1.502902000	3.821074000
1	-2.691135000	0.752960000	4.600793000
1	-2.586372000	2.489495000	4.210746000
1	-3.904239000	1.499038000	3.529937000
7	-1.351412000	0.935220000	1.777270000

Table S3. XYZ-coordinates for the *trans*-$[C_{20}H_{22}FeN_{10}O]^{3+}$ species (charge 3, multiplicity 2, G° = -2677.89938 h)

8	1.173961000	0.004506000	1.716722000
7	2.852428000	1.099514000	0.565486000
7	2.860948000	-1.083058000	0.571658000
7	1.051169000	-2.705720000	0.205496000
7	-0.988239000	-2.779436000	-0.442742000
7	-2.606082000	-1.083742000	-1.042075000
7	-2.617679000	1.054774000	-1.034960000
7	-1.015394000	2.764204000	-0.435196000
7	1.028974000	2.707326000	0.199515000
6	2.243229000	0.007065000	1.046803000
6	3.914442000	0.685835000	-0.249768000
1	4.605043000	1.384216000	-0.701384000
6	3.919557000	-0.665882000	-0.246225000
1	4.615386000	-1.361399000	-0.694190000
6	2.317726000	-2.388073000	0.893959000
1	2.145908000	-2.424534000	1.970885000
1	3.044496000	-3.152204000	0.621205000
6	-0.107931000	-1.992871000	0.197040000
6	0.863385000	-3.938466000	-0.405704000
1	1.648306000	-4.678742000	-0.478183000
6	-0.419409000	-3.987361000	-0.817412000
1	-0.971905000	-4.766699000	-1.323522000
6	-2.395124000	-2.460992000	-0.611036000
1	-2.918267000	-2.622385000	0.335300000
1	-2.812664000	-3.126741000	-1.366981000
6	-1.943031000	-0.012507000	-0.571591000
6	-3.705622000	-0.691590000	-1.796536000
1	-4.375578000	-1.399114000	-2.265084000
6	-3.712937000	0.655946000	-1.792081000
1	-4.390369000	1.359262000	-2.256190000
6	-2.419848000	2.430977000	-0.594833000
1	-2.851264000	3.097581000	-1.342174000
1	-2.937157000	2.579005000	0.356840000
6	-0.123508000	1.983854000	0.195691000
6	-0.460513000	3.978811000	-0.808797000
1	-1.023422000	4.754443000	-1.309117000
6	0.825269000	3.940811000	-0.405381000
1	1.602735000	4.688643000	-0.480664000
6	2.301580000	2.402274000	0.882980000
1	3.021445000	3.169903000	0.601817000
1	2.135034000	2.444172000	1.960575000
26	-0.298773000	-0.004739000	0.467795000
7	-1.371112000	-0.001821000	2.069778000
6	-1.865492000	0.011072000	3.102395000
6	-2.471918000	0.029117000	4.419705000
1	-2.156076000	0.929758000	4.952903000
1	-3.561151000	0.022860000	4.330858000
1	-2.148322000	-0.851293000	4.981308000
7	0.742324000	-0.002927000	-1.233782000
6	1.222187000	-0.002342000	-2.274853000
6	1.826196000	-0.002155000	-3.594344000
1	2.439232000	-0.898132000	-3.720763000
1	1.042793000	0.006367000	-4.356979000
1	2.452722000	0.885274000	-3.714638000

6. References

[1] Olmstead, M. M.; Power, P. P.; Shoner, S. C., *Inorg. Chem.* **1991,** *30* (11), 2547-2551.

[2] Shine, H. J.; Zhao, B.-J.; Marx, J. N.; Ould-Ely, T.; Whitmire, K. H., *J. Org. Chem.* **2004,** *69* (26), 9255-9261.

[3] Anneser, M. R.; Haslinger, S.; Pöthig, A.; Cokoja, M.; Basset, J.-M.; Kühn, F. E., *Inorg. Chem.* **2015,** *54* (8), 3797-3804.

[4] Sniekers, J.; Verguts, K.; Brooks, N. R.; Schaltin, S.; Phan, T. H.; Trung Huynh, T. M.; Van Meervelt, L.; De Feyter, S.; Seo, J. W.; Fransaer, J.; Binnemans, K., *Chem. Eur. J.* **2016,** *22* (3), 1010-1020.

[5] Bass, H. M.; Cramer, S. A.; McCullough, A. S.; Bernstein, K. J.; Murdock, C. R.; Jenkins, D. M., *Organometallics* **2013,** *32* (7), 2160-2167.

[6] Kaub, C.; Lebedkin, S.; Bestgen, S.; Köppe, R.; Kappes, M. M.; Roesky, P. W., *Chem. Comm.* **2017,** *53* (69), 9578-9581.

[7] Kück, J. W.; Anneser, M. R.; Hofmann, B.; Pöthig, A.; Cokoja, M.; Kühn, F. E., *ChemSusChem* **2015,** *8* (23), 4056-4063.

[8] F. Neese, *WIREs Comput. Mol. Sci.* **2012**, *2*, 73-78.

[9] S. Lehtola, C. Steigemann, M. J. T. Oliveira, M. A. L. Marques, *SoftwareX* **2018**, *7*, 1-5.

[10] E. F. Valeev, Libint: A library for the evaluation of molecular integrals of many-body operators over Gaussian functions **2020**

[11] J.-D. Chai, M. Head-Gordon, *J. Chem. Phys.* **2008**, *128*, 084106.

[12] S. Grimme, J. Antony, S. Ehrlich, H. Krieg, *J. Chem. Phys.* **2010**, *132*, 154104.

[13] F. Weigend, R. Ahlrichs, *Phys. Chem. Chem. Phys.* **2005**, *7*, 3297-3305.

[14] F. Weigend, *Phys. Chem. Chem. Phys.* **2006**, *8*, 1057-1065.